Sustainable Energy & Fuels

Interdisciplinary research for the development of sustainable energy technologies

Accepted Manuscript

This article can be cited before page numbers have been issued, to do this please use: S. Kumar, M. Myekhlai, S. Lim and H. Oh, *Sustainable Energy Fuels*, 2026, DOI: 10.1039/D5SE01539A.

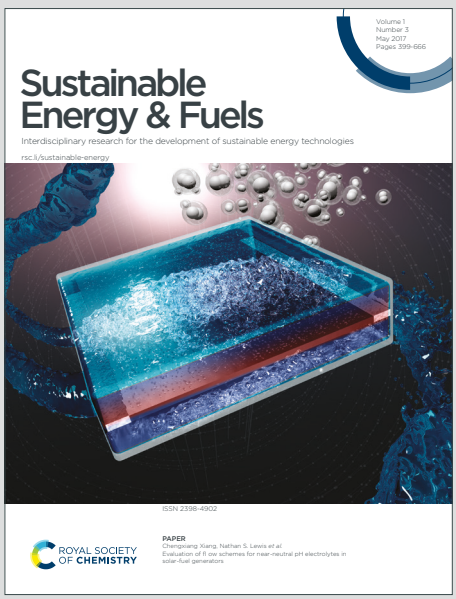

ROYAL SOCIETY OF CHEMISTRY

rsc.li/sustainable-energy

View Article Online
DOI: 10.1039/D5SE01539A

Understanding Factors Affecting Storage Capacity and Reproducibility in Realistic Ambient-Temperature Hydrogen Physisorption

Sandeep Kumar,[a*] Munkhshur Myekhlai,[a] Subin Lim,[a] and Hyunchul Oh[a,b*]

[a] Department of Chemistry, Ulsan National Institute of Science and Technology (UNIST), Ulsan, Republic of Korea

[b] Graduate School of Carbon Neutrality, Ulsan National Institute of Science and Technology (UNIST), Ulsan, Republic of Korea

*Email; chem.skumar7@unist.ac.kr / hcoh@unist.ac.kr

Abstract: Physisorption-based materials such as metal-organic frameworks (MOFs), covalent organic frameworks (COFs), and porous carbons have been extensively studied for hydrogen storage due to their high surface areas and tunable pore structures. While these materials show high hydrogen uptake at cryogenic temperatures, storage at ambient conditions (0–50 °C) remains challenging due to weaker binding energies. To improve ambient-temperature performance, various approaches, including metal doping, pore engineering, and functionalization, have been explored. However, some reported ambient-temperature uptake values approach those seen only at cryogenic conditions, raising concerns about measurement errors and reproducibility. This review highlights these challenges and stresses the need for standardized experimental protocols and transparent data sharing. By minimizing errors and fostering reproducibility, future research can accelerate the development of practical, scalable hydrogen storage technologies operable at near-ambient conditions.

Keywords: Room temperature H_2 storage, porous materials, MOFs, Porous carbon, COFs

View Article Online
DOI: 10.1039/D5SE01539A

1. Introduction

Rapid urbanization and industrialization have made environmental pollution a major global concern, particularly the rising atmospheric carbon concentration [1,2]. The primary contributor to this issue is the combustion of fossil fuels, which releases large amounts of carbon into the environment. Moreover, fossil fuel reserves are depleting rapidly, underscoring the urgent need for sustainable alternatives [3–6]. Among the various energy options, hydrogen as a fuel has gained significant attention due to its high energy density, abundant availability, and carbon-free utilization[7,8]. As the world transitions toward a low-carbon future, hydrogen offers a promising pathway to reduce greenhouse gas emissions and serve as a clean, sustainable alternative to fossil fuels. However, hydrogen energy systems still face critical challenges related to storage efficiency, transportation, and safety, which limit their large-scale application[9,10]. The low volumetric energy density of hydrogen makes storage difficult, necessitating high-pressure compression and cryogenic liquefaction, each of which introduces additional complexity, cost, and energy loss. Safety is another major concern, as hydrogen's small molecular size increases the risk of leakage, its wide explosion range (volume ratio of 11-59%), and its wide flammability range heighten the risk of accidental ignition[11]. Hydrogen-induced cracking often occurs in conjunction with stress corrosion cracking (SCC), and their combined effects can lead to severe material degradation and eventual pipeline failure[12]. Moreover, storage remains challenging, demanding cryogenic temperatures (20.15 K) or high pressures (up to 700 bar)[13,14].

Addressing these challenges requires the development of advanced methods, optimized system designs, and stringent safety protocols to enable efficient, secure, and practical hydrogen storage solutions for a sustainable energy future. Hydrogen storage strategies generally fall into two categories: physical methods-such as compression, cryo-compression,

View Article Online
DOI: 10.1039/D5SE01539A

and liquid hydrogen, and material-based methods involving chemical or physical adsorption [15,16]. In physical-based storage, H_2 storage via high-pressure compression is a common method [17,18]. It involves compressing H_2 gas to extremely high pressures (typically 200-700 bar) and storing it in specialized high-pressure tanks. While cryogenic liquefaction of H_2, by which the H_2 gas will be cooled to its liquefaction temperature (20 K) in a container[19,20]. Both methods can store hydrogen efficiently but face long-term application issues, high maintenance costs, and handling issues. Materials-based chemical hydrogen storage primarily involves metal hydrides, liquid organic hydrogen carriers, and other chemical hydrogen systems, all of which depend on the formation and breaking of chemical bonds during hydrogen uptake and release. In contrast, physisorption-based storage using high-surface-area porous materials has emerged as a significant research focus due to its reversible, weakly bound adsorption mechanisms and potential for rapid kinetics.

Physisorption-based storage offers several key benefits for hydrogen energy applications[21]. In this way, hydrogen is stored via weak intermolecular (van der Waals) forces. It operates under relatively mild temperature and pressure conditions, making it safer and more energy-efficient than high-pressure or cryogenic storage methods[22,23]. The process is reversible, allowing for easy hydrogen adsorption and desorption without significant structural degradation of the storage material[24]. Materials such as metal–organic frameworks (MOFs), activated carbons, covalent organic frameworks (COFs), and zeolites provide high surface areas and tunable pore structures, enabling enhanced hydrogen uptake via physisorption. Additionally, these materials can be engineered to improve adsorption properties through functionalization or pore size optimization, making them attractive for lightweight and portable hydrogen storage systems[25,26]. Despite these advantages, physisorption-based storage technologies also face some limitations. The weak van der Waals interactions between

View Article Online
DOI: 10.1039/D5SE01539A

hydrogen molecules and the adsorbent result in low binding energies, leading to poor storage capacities at ambient temperatures. Consequently, efficient hydrogen adsorption often requires cryogenic conditions, increasing system complexity and cost. Furthermore, maintaining material stability and consistent performance over repeated cycles remains challenging. The scalability, synthesis cost, and mechanical integrity of adsorbent materials also limit their practical deployment. To overcome these issues, future research must focus on enhancing adsorption strength, improving thermal management, and developing cost-effective, high-capacity materials for real-world hydrogen storage applications.

This review focuses on hydrogen uptake using adsorbent materials at 0–50°C and pressures up to 200 bar. It emphasizes key aspects such as reproducibility, long-term cycle stability, current challenges, and future prospects. While most research on physisorbed hydrogen storage has been conducted at 77 K, this review aims to address performance at near-ambient temperatures. In addition, the reproducibility of hydrogen storage measurements in porous materials is a significant challenge due to variations in synthesis, activation, and measurement conditions, including pressure, temperature, and calibration. Furthermore, moisture sensitivity and structural differences (particularly in metal-organic frameworks, MOFs) can affect consistency. Round-robin studies have reported a 20–40% variation in hydrogen uptake for the same material under similar conditions. Therefore, this review will highlight these issues to guide the design of materials and the development of experimental approaches that could enhance recyclability.

2. **Fundamentals of Physisorption-Based Hydrogen Storage**

Hydrogen molecules behave differently for physisorption, chemisorption, and weakly bonded hydrogen storage methods (quasi-molecular interactions, such as Kubas interactions) (**Fig.**

View Article Online
DOI: 10.1039/D5SE01539A

1)[27,28]. The binding enthalpy of each method depends on the interaction of hydrogen with the surface (Table 1). The change in the behavior of hydrogen molecules during the adsorption and the potential energy are shown in **Fig. 1**.

Table 1: Comparison of binding strength of hydrogen storage[26].

	Physisorption	Chemisorption	Kubas interaction
Binding enthalpy (kJ/mol)	-4 – -10	-100 – -200	-20 – -70

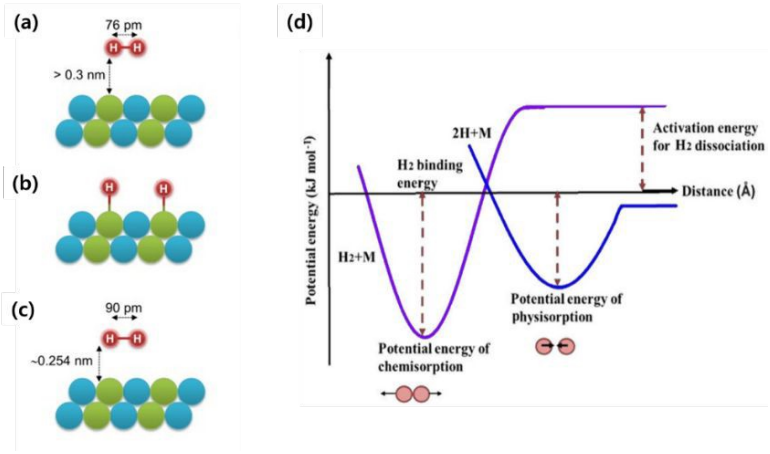

Fig. 1. (a) Physisorption, (b) chemisorption, (c) weakly bonded hydrogen[29], (Reproduced from ref. 29 with permission from Wiley, copyright 2015), and (d) One-dimensional potential energy profiles for physisorption and chemisorption processes plotted as a function of the separation distance between H_2 molecules and the substrate. Reprinted with permission [25], (Reproduced from ref. 25 with permission from Wiley, copyright 2025)

Physisorption-based hydrogen storage involves three main steps: (i) mass transfer of hydrogen molecules to the material surface, (ii) diffusion into internal pores or structures, and (iii) rapid adsorption onto internal surfaces. Since the final adsorption step is very fast, the overall kinetics are controlled primarily by the first two steps (**Fig. 2**)[30]. The process relies mainly on weak van der Waals forces between hydrogen molecules and the surfaces of porous materials like MOFs, COFs, or activated carbons.[31]. Adsorption begins with monolayer formation,

View Article Online
DOI: 10.1039/D5SE01539A

sometimes followed by multilayer adsorption, favoring materials with high specific surface areas and slit-shaped nanopores. The total hydrogen storage capacity includes both surface adsorption and compression within pore voids. High surface area and optimized microstructure are critical for enhancing storage performance. Hydrogen remains molecular during adsorption, without forming chemical bonds, enabling reversible adsorption and desorption [32] [33] [34] [35]. Thus, this physisorption mechanism enables rapid hydrogen uptake and release, facilitating quick refueling. The adsorption/desorption processes involve low enthalpy changes (typically 1–10 kJ/mol), which ease thermal management and minimize heat transfer challenges. Moreover, since no chemical reactions occur, hydrogen storage preserves the gas without loss from side reactions [16].

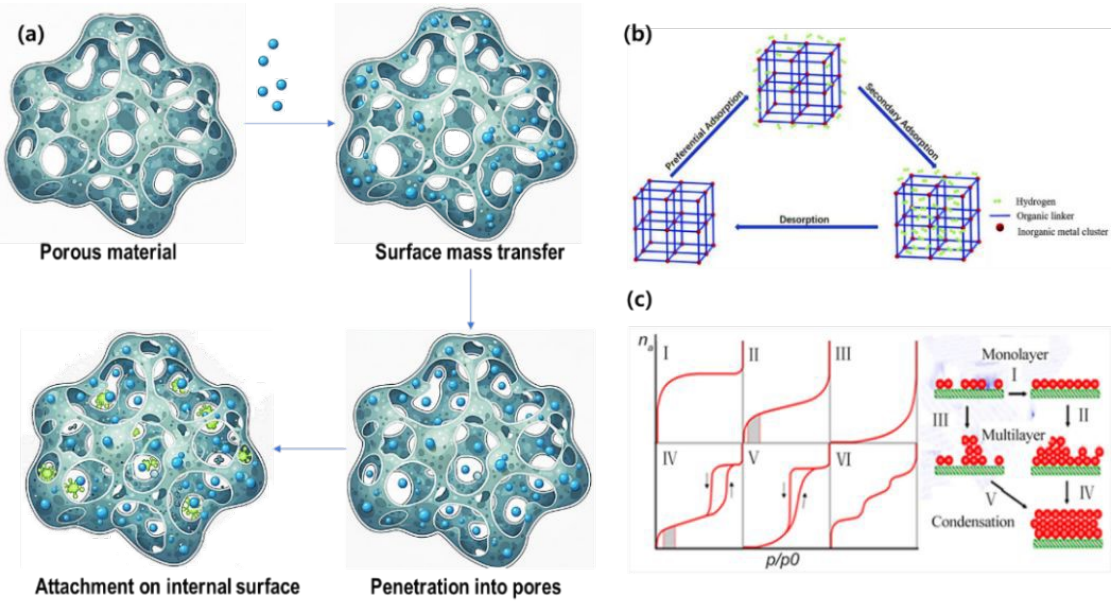

Fig. 2. (a) Illustration of the mechanism of hydrogen adsorption in porous materials, (b) hydrogen storage mechanism in MOFs[36] (Reproduced from ref. 36 with permission from Elsevier, copyright 2024), and (c) different types of adsorption isotherms[37]. (Reproduced from ref. 37 with permission from Scientific Research, copyright (open access) 2018)

Particularly in MOFs, hydrogen transport is primarily governed by adsorption and self-diffusion processes. The unique porous structure of MOFs arises from coordination between

View Article Online
DOI: 10.1039/D5SE01539A

metal clusters and organic linkers (**Fig. 2b**)[38], creating distinct adsorption sites. Hydrogen predominantly adsorbs at inorganic metal clusters, such as Zn_4O in MOF-5, with weaker adsorption near oxygen coordination and organic linker sites. Experimental and computational studies confirm that metal oxide clusters serve as the main active sites for hydrogen adsorption, while organic linkers contribute secondary, weaker binding sites.[36,39].

Hydrogen adsorption is effectively described by adsorption isotherms, which show the relationship between the quantity of adsorbed hydrogen and pressure at constant temperature. At low pressures, adsorption occurs rapidly on high-energy sites, while at higher pressures, multilayer adsorption leads to saturation. Comparing isotherms at different temperatures reveals that lower temperatures enhance adsorption due to stronger van der Waals forces. According to IUPAC (**Fig. 2c**), adsorption isotherms are classified into six types. For hydrogen storage in porous materials, Type I (Langmuir) isotherms dominate; these characterize microporous materials such as MOFs, zeolites, and activated carbons, where adsorption quickly saturates the micropores. Type II and IV isotherms are linked to mesoporous materials exhibiting multilayer adsorption or capillary condensation. Other types (III, V, VI) are rare for hydrogen but relate to weak adsorbent-adsorbate interactions or layer-by-layer adsorption. Understanding isotherm types helps identify pore structures and adsorption behaviors, which are critical for optimizing hydrogen storage materials[37,40].

Efficient hydrogen storage using porous adsorbents depends on multiple interrelated material and operational factors. First, hydrogen uptake capacity must be considered both gravimetrically (wt%) and volumetrically (g/L)[41], as these metrics impact suitability for mobile and stationary applications, respectively. Gravimetric capacity determines how much hydrogen can be stored per unit mass, which is critical for weight-sensitive uses like fuel cell vehicles, while volumetric capacity defines the total storage per unit volume, essential for

View Article Online
DOI: 10.1039/D5SE01539A

confined or fixed systems. Moreover, understanding the distinction between excess and total adsorption is vital in hydrogen adsorption studies. Excess adsorption describes the amount of gas taken up by the material beyond what would normally occupy the pore volume at the bulk gas density, and this is the value most commonly obtained from experimental measurements. Total (or absolute) adsorption, however, reflects the full amount of gas present inside the pores, including both the adsorbed molecules and the free gas corresponding to the bulk density. Although the difference between these two quantities is negligible at low pressures, it becomes increasingly important at high pressures-especially near ambient temperature, where the bulk gas density rises sharply, and excess adsorption alone can underestimate the true storage capacity. Thus, differentiating excess from total adsorption is essential for accurately assessing and comparing the high-pressure hydrogen storage capabilities of porous materials[42].

The total amount of hydrogen adsorbed is fundamentally governed by the material's pore geometry, size, and surface area[43]. Microporous materials with pore diameters below roughly 9 Å and a large specific surface area maximize hydrogen uptake, since they offer more adsorption sites and optimal confinement [42][33,44–46]. However, because physisorption relies on weak van der Waals forces, practical hydrogen storage is typically optimized at either low temperatures or high pressures, which presents engineering and operational challenges for real-world deployment. Adsorption enthalpy is another essential variable that influences the strength and reversibility of the hydrogen–adsorbent interaction. Under cryogenic conditions, uptake at low pressure is dictated by enthalpy, while surface area and pore volume become more important at higher pressures[41][47]. To further improve hydrogen storage capacity, materials can be tailored by adjusting pore shape, increasing specific surface area, exchanging light metal components, or modifying the microstructure [48]. For example, slit-shaped pores in carbon-based materials or tailored pore architectures in MOFs enable higher gravimetric uptake

View Article Online
DOI: 10.1039/D5SE01539A

compared to tubular or spherical pores (**Fig. 3**). Finally, efficient hydrogen adsorbents must also exhibit reversibility and cycle stability, maintaining performance across repeated charging and discharging cycles. Ultimately, optimizing pore shape, size, connectivity, and composition is critical for balancing gravimetric and volumetric hydrogen uptake, enabling high-performance and practical hydrogen storage systems.

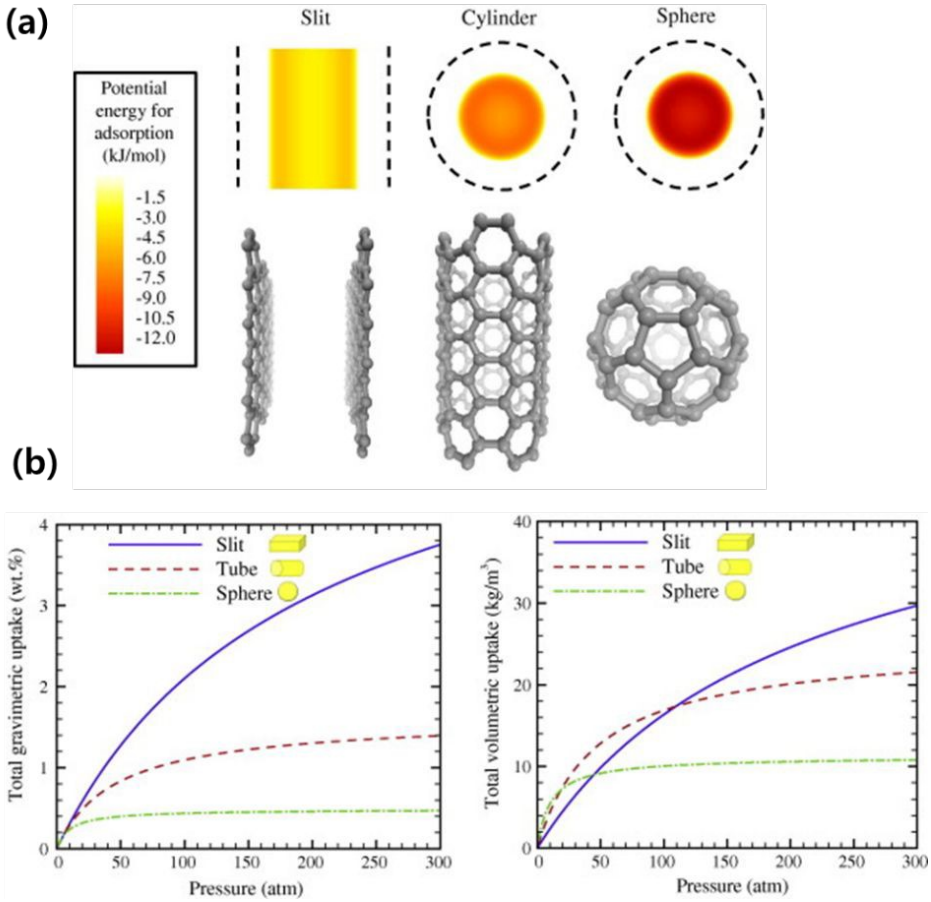

Fig. 3. (a) Types of pores and (b) effect of different pore structures on the gravimetric and volumetric uptake of hydrogen with a dimension of 10 Å and at a temperature of 243 K. Reprinted with permission [48], Copyright 2013 Elsevier (Reproduced from ref. 48 with permission from Elsevier, copyright 2013)

To ensure practical progress in hydrogen storage technology, researchers commonly benchmark their work against established targets set by organizations like the U.S. Department of Energy (DOE). For instance, the DOE's 2025 technical targets for onboard hydrogen storage

View Article Online
DOI: 10.1039/D5SE01539A

in light-duty vehicles call for a gravimetric capacity of 5.5 wt% and a volumetric capacity of 40 g/L[49,50]. Achieving both high gravimetric and volumetric storage simultaneously remains challenging, as improvements in one often compromise the other [36]. Another core parameter is the adsorption enthalpy (ΔH_{ads}), which quantifies the interaction strength between hydrogen molecules and the storage material's surface. This value directly influences how readily hydrogen can be adsorbed or desorbed at given temperatures (T1 & T2) and pressures (P_1 & P_2). Typically, the isosteric heat of adsorption (Q_{st}) is calculated from hydrogen isotherms at multiple temperatures using the Clausius–Clapeyron relation[51]:

$$Q\square\square = -R \times [\ln(P_2 / P_1)] / [(1/T_2) - (1/T_1)]$$

where R is the gas constant. The adsorption enthalpy is then $\Delta H\_ads = -Q_{st}$, reflecting the exothermic nature of physisorption. The physisorption enthalpy typically falls within 1–10 $kJ \cdot mol^{-1}$. Precise measurement of ΔH_{ads} requires careful control of temperature, pressure, and sample activation, as small experimental deviations can lead to significant errors. For practical use, an ideal physisorption material should have moderate adsorption enthalpies (strong enough for stable storage near ambient conditions, yet weak enough for fast hydrogen release). Both storage temperature and pressure significantly affect usable capacity and kinetics: lower temperatures favor adsorption, while higher temperatures support desorption (**Fig. 4**)[52]. Thus, identifying optimal T–P windows that balance storage efficiency and reversibility is essential for practical hydrogen storage applications[53].

View Article Online
DOI: 10.1039/D5SE01539A

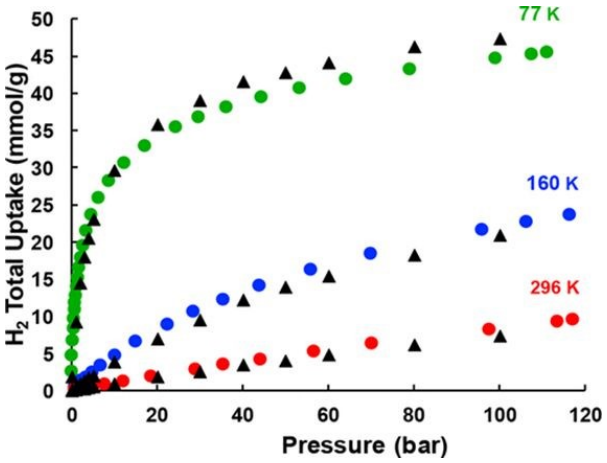

Fig. 4. Experimental (circles) and simulated (triangles) total hydrogen adsorption isotherms at 77 K (green), 160 K (blue), and 296 K (red) for NU-125[52]. (Reproduced from ref. 52 with permission from The American Chemical Society, copyright 2018)

Beyond capacity and energetics, real-world hydrogen storage solutions must be durable and reproducible. Regenerability and cycle stability are key: materials must maintain performance over repeated adsorption–desorption cycles. However, operational realities (like experimental variability, equipment calibration, and surface changes) can reduce storage capacity over time. Degradation mechanisms, including pore-blocking, structural changes, or contamination, must be minimized. Therefore, standardized testing and careful experimental control are essential to evaluate and guarantee long-term stability, which is critical for the deployment of hydrogen storage in transportation and industry.

While considerable hydrogen storage research has focused on very low temperatures, evaluating materials within the 0–50 °C range is particularly important for real-world applications. This moderate temperature window closely matches conditions commonly encountered in indoor environments, laboratory testing, and vehicle interiors during standard use. Focusing on this range enables reliable assessment of material performance without the high energy cost or engineering complexity of extreme thermal management[54], and greatly

View Article Online
DOI: 10.1039/D5SE01539A

increases the relevance and practicality of storage solutions for onboard, portable, and industrial hydrogen energy systems.

3. **Adsorbent at Near Ambient Temperature and ≤ 200 bar**

Porous materials continue to attract attention for H_2 storage due to their fast kinetics, higher operating temperatures than LH_2, and lower pressures than those of compressed tanks [55–58]. They can store H_2 over a range of temperatures and pressures and can be easily modified to optimize conditions. Additionally, these materials offer a safer alternative to other H_2 storage methods. Adsorption-based H_2 storage at ambient temperature primarily uses materials such as activated carbon, carbon nanotubes, zeolites, covalent organic frameworks (COFs), and metal-organic frameworks (MOFs)[59–64]. These materials have high surface areas and pore volumes, enabling effective physical adsorption of H_2. In the following sections, we will summarize the MOFs, porous carbon materials, and COFs used for efficient H_2 storage at ambient temperature.

3.1. Carbon-Based Materials

Carbon-based materials[65], including graphene[66], activated carbons (ACs)[67,68], carbon nanotubes (CNTs)[69,70], mesoporous carbons[71], and carbon nitrides[72,73], have been extensively studied for ambient-temperature H_2 storage because of their abundant resources, thermal and chemical stability, high specific surface area, and porous structure. However, the H_2 adsorption energy on carbon adsorbents is relatively low, at approximately 5 kJ/mol [74,75]. As a result, to improve the hydrogen storage capacity of carbon nanostructures, the main strategies include enhancing the specific surface area[70,76], developing well-defined microporosity[65,77], and increasing the hydrogen adsorption energy[67,78]. The following sections will provide a detailed discussion of recent advancements in the development of widely used carbon structures, exploring their potential for room temperature hydrogen storage.

Graphene structures have been examined as H_2 storage materials owing to their two-

View Article Online
DOI: 10.1039/D5SE01539A

dimensional layered structure and adjustable textural properties[65,66,77]. However, the interlayer distance in graphene is 3.5 Å, limiting its ability to accommodate H_2 molecules. Thus, experimental studies have been performed to increase the H_2 uptake of graphene structures by optimizing their d-spacing, porosity, and binding energy[66,77]. **Table 2** presents a summary of graphene and graphene oxide samples modified by optimizing interlayer distance and porosity to improve room temperature hydrogen storage. The modified graphene and graphene oxide samples exhibited hydrogen uptakes from 1.34 to 4.65 wt% at ambient temperature. The interlayer distance of graphene has been increased to 6-7 Å in graphene oxide, which is assumed to be optimal for storing H_2 molecules. For instance, *Rajaura et al.,* investigated that Graphene oxide (GO) shows 1.9 wt.% H_2 adsorption at ambient temperature and 80 bar, higher than the 1.34 wt.% of reduced graphene oxide (r-GO). This enhanced uptake is presumed to result from GO's larger interlayer distance of 8.84 Å compared to 3.85 Å for r-GO.[66]. Furthermore, *Yadav et al.* studied the effect of the alignment and interlayer spacing of graphene layers on H_2 uptake by using different pretreatment temperatures. Graphene oxide (GO) preheated at 400 °C showed about 2.5 wt.% H_2 uptake at room temperature and 20 bar, higher than samples treated at lower temperatures. The enhanced storage is likely related to optimized interlayer spacing (6–7.5 Å) and improved alignment (**Fig. 5**)[77]. *Kim et al.* synthesized mesoporous graphene oxide using hydrothermal treatment. Mesoporous GO prepared hydrothermally exhibited 4.65 wt.% H_2 uptake at 40 bar, presumably due to enlarged interlayer spacing and mesoporosity facilitating H_2 diffusion[65]. However, maintaining an optimal interlayer distance alone may not yield such high ambient-temperature uptake, as physisorption energies on GO are typically low (<10 kJ mol^{-1}). Reported values could also reflect experimental uncertainties, contributions from chemisorption, or measurement under non-equilibrium conditions rather than true reversible physisorption capacity.

View Article Online
DOI: 10.1039/D5SE01539A

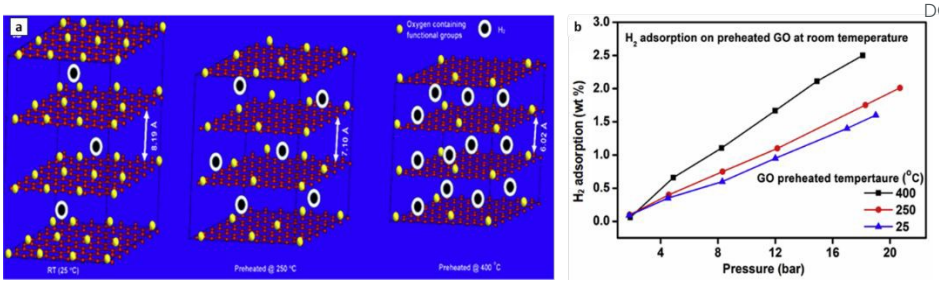

Fig. 5. The effect of interlayer distance of GO on H_2 adsorption (a) the control of interlayer spacing by altering the pretreatment temperature, (b) the H_2 adsorption properties of GO samples with different interlayer distances[77]. (Reproduced from ref. 77 with permission from Elsevier, copyright 2020)

In addition, Metal nanoparticle decoration **(Fig. 6)**, such as with transition metals, metal borides, or alloys, is considered to enhance H_2 adsorption in graphene by modifying the binding energy and potentially altering the storage mechanism [79–85]. Reported studies suggest that graphene decorated with Ni–B[81] or Pd nanoparticles[82] exhibits markedly higher H_2 uptake (up to about 8 wt% at RT, 60 bar) than pristine graphene, possibly due to spillover effects and increased interaction with H_2 molecules. However, H_2 uptakes exceeding 2 wt%@100 bar at ambient conditions should be interpreted with caution, as their reproducibility requires rigorous verification. Because carbon materials are lightweight, even small measurement errors can lead to significant deviations in gravimetric values. In addition, chemically bonded H_2 at dangling bonds or defect sites may contribute irreversibly to measured capacities, complicating interpretation[86–88]. Several experimental studies have attempted to reproduce such high uptake values, but many have reported inconsistent or irreproducible results, suggesting that earlier findings may be influenced by experimental artifacts or non-equilibrium adsorption effects[86,87,89–92]. Therefore, repeatability tests and independent validation under well-defined equilibrium conditions are essential to confirm genuine physisorption-based storage performance.

View Article Online
DOI: 10.1039/D5SE01539A

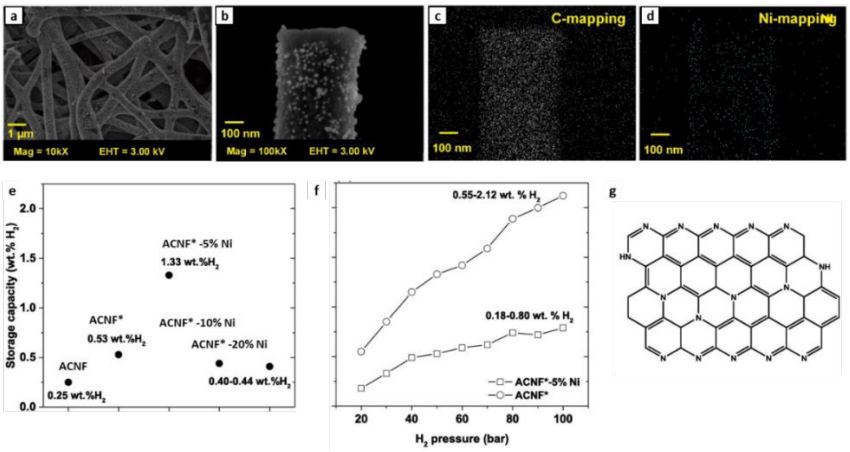

Fig. 6. Improving the H_2 adsorption of activated carbons via metallic nanoparticle decoration. (a-d) SEM images and EDX-mappings of 5 wt% Ni-doped ACNFs, (e-f) H_2 adsorptions at RT of ACNFs with and without Ni-doping with different Ni content, and (g) chemical structure of ACNF[67]. (Reproduced from ref. 67 with permission from Elsevier, copyright 2021)

Carbon nanotubes (CNTs) have also been studied for hydrogen storage due to their tubular structures offering internal and external adsorption sites[93–95]. However, their relatively low surface area and weak adsorption energy restrict their H_2 uptake, which typically ranges below 1 wt% at ambient temperature. Efforts have focused on increasing surface area and microporosity through chemical activation, such as KOH treatment, to improve storage performance[96,97]. Some reports have described CNTs with very high surface areas and up to about 4 wt% H_2 uptake [70,98–100], but such results are likely influenced by specific synthesis or activation conditions [101] and require further verification to confirm reproducibility under equilibrium conditions.

Heteroatom doping and metal decoration are considered potential methods to enhance the H_2 adsorption capacity of CNTs by increasing adsorption energy. Incorporation of boron (B) or nitrogen (N) into the CNT framework can modify charge distribution and strengthen interactions with H_2 molecules [102–104]. Some studies have reported enhanced uptake, such as about 0.5 wt% for B-doped CNTs at 273 K and 1.6 MPa, and up to 2 wt%@100bar for N-doped CNTs at ambient conditions[105][104]. However, these improvements likely depend on synthesis

View Article Online
DOI: 10.1039/D5SE01539A

conditions and dopant levels, and subsequent works have shown inconsistent or lower H_2 uptakes [106,107], possibly due to tube blockage or structural defects formed during doping.

Table 2: Carbon-based adsorbents exhibiting more than 1 wt% of H_2 uptake at RT

Sr. No.	Materials	BET SSA / m^2 g^{-1}	Pressure / Bar	H_2 uptake / wt%	Ref.
1	**GO/MWCNT**	-	50	2.6	[69]
2	**Mesoporous GO**	120	40	4.65	[65]
3	**GO**	-	80	1.90	[66]
4	**rGO**	-	80	1.34	[66]
5	**Preheated self-aligned GO**	-	20	2.5	[77]
6	**Rice husk-derived graphene**	315.07	30	1.95	[108]
7	**1 % Pd/GN**	-	60	8.67	[82]
8	**5 % Pd /GN**	-	60	7.16	[82]
9	**Pd/N-SG**	-	40	4.3	[81]
10	**Pd_3Co-NG**	-	30	4.20	[83]
11	**CoB decorated graphene**	-	-	2.68	[85]
12	**Mn-V /GN**	326	40	1.81	[109]
13	**Pt/GN foam**	290.98	100	3.19	[79]
14	**Ni-B nanoalloy / GN**	272	1	1.9	[84]
15	**Ni-Ti-Mg/B-GN**	-	-	6.4	[80]
16	**Ca/GN**	-	-	5	[110]
17	**Ni/porous graphite**	95	10	4.48	[111]
18	**Ni/porous graphene**	925	5	1.95	[112]
19	**MgNi/NG**	678.5	30	5.4	[113]
20	**CNTs, CN4-800**	3802	150	4.4	[70]
21	**Co-doped CNT**	-	1	1.51	[99]
22	**rGO-MWCNT**	-	50	2.1	[69]
23	**N/CNT**	870	100	2.0	[104]
24	**Ti-MWCNT**	237	20	1.88	[114]
39	**Sc/ND-CNT**	-	-	5.85	[100]
40	**Endohedral Ni atoms on SWNT**	-	-	2.91	[115]
41	**Au-doped CNTs**	-	-	3.42-5	[78]
42	**Li-PCNT**	-	-	2.13	[116]
43	**Nanotube-fullerene**	-	-	7.7	[117]
44	**Packed SWCNTs**	-	-	5.5	[118]
26	**MWTSC-50-3-700**	1785	40	4.73	[76]
27	**B-Carbon**	-	100	5.9	[119]
28	**Ni-doped activated carbon nanofibers**	-	10	2.12	[67]
29	**Ni-doped N/O-rich hierarchical porous carbon**	-	100	2.4	[120]
30	**Pt /AX21**	-	100	1.2	[121]
31	**Ru/templated C (TC)**	-	103	1.43	[122]
32	**Pt/ TC**	-	103	1.3	[122]
33	**Pt-ACs-MOF-5**	730	100	2.3	[68]
34	**MgH_2-Ni/CMK**	-	30	3.9	[71]
35	**g-C_3N_4**	28.8	30	1.8	[73]
36	**Pd_3Co-gC_3N_4**	36.6	30	5.3	[73]
37	**g-C_3N_4**	28.8	40	2.6	[72]
38	**Pd-g-C_3N_4**	26.8	40	3.4	[72]
45	**Single-atom Pt@C_{60-x}**	202.8	100	6.8	[123]

View Article Online
DOI: 10.1039/D5SE01539A

However, a plausibility check for exceptional RT claims in Table 2 is necessary. At 298 K, most porous carbons typically show sub-1 wt% excess uptake below ~100 bar, and even the best chemically activated carbons reach ~1–3 wt% only at much higher pressures (tens of MPa). Therefore, the exceptionally high values in Table 2 (*e.g.*, ≥4 wt% at ≤100 bar, and particularly several g-C3N4-based or metal-decorated samples showing 4–9 wt%) should be interpreted with caution. Potential causes include (i) inconsistent reporting basis (excess vs total/absolute uptake), (ii) uncertainties in buoyancy/dead-volume corrections under high pressure, (iii) incomplete degassing or moisture/impurity effects, and (iv) irreversible contributions from metal sites (chemisorption/hydride-like uptake) that do not translate into reversible physisorption capacity. While metal intercalation or doping is known to enhance the hydrogen uptake of activated carbons at ambient temperature, the results can be inconsistent. For instance, the hydrogen adsorption for palladium (Pd)-decorated activated carbon was measured at 0.38 wt% at 50 bar, which is lower than the 0.58 wt% observed for regular activated carbon under the same conditions. This decrease in adsorption was attributed to pore blockage by Pd nanoparticles, resulting in a reduced specific surface area and, consequently, a lower hydrogen uptake[124]. The surface-area–uptake correlation shown in **Fig. 7** is used here as a first-pass sanity check rather than a strict theoretical limit, because classical surface-area scaling (e.g., Chahine-type correlations) was originally established for 77 K excess uptake. At room temperature, micropore volume/ultramicropore distribution and reporting methodology can dominate the apparent uptake, and thus outliers require careful validation. In particular, a high-surface-area CNT sample was reported to show ~4.4 wt% uptake; however, given the typical RT uptake range for porous carbons, such a value should be treated as an outlier unless independently validated with clearly stated uptake definitions (excess vs. total) and rigorous high-pressure corrections.

View Article Online
DOI: 10.1039/D5SE01539A

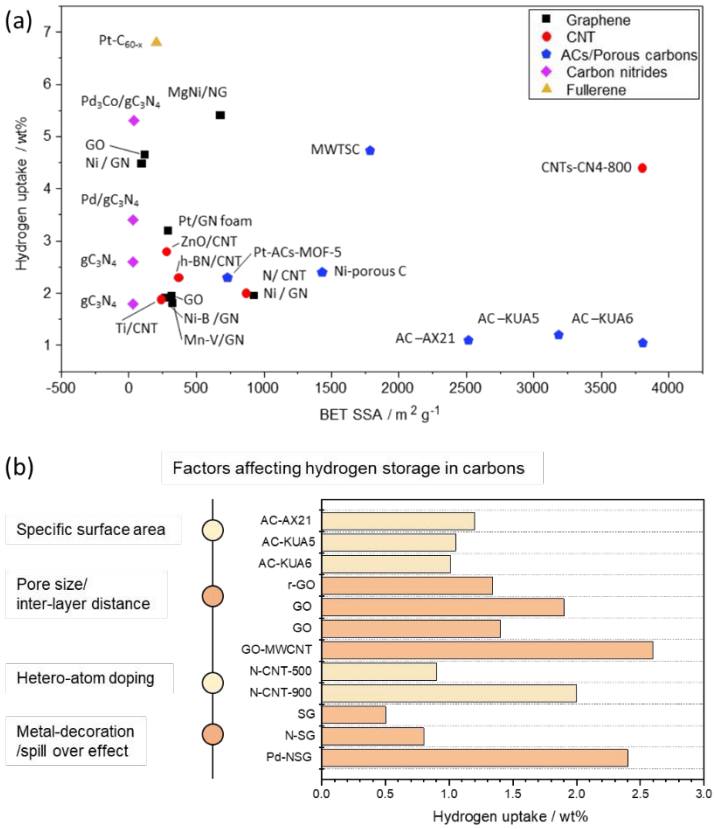

Fig. 7. (a) Comparison of the H_2 storage capacities of carbon-based adsorbents with respect to their specific surface area and (b) factors affecting the hydrogen storage in carbon-based materials.

Theoretical studies suggest that carbon nanotubes (CNTs) could achieve higher hydrogen uptake when *idealised* tube packing, diameter, and metal doping are assumed[78,118,125,126]. For example, a 6 wt.% uptake at 1 MPa and 77 K was predicted for optimised single-walled CNT packing [126], while GCMC simulations reported 6.5 wt.% at 300 K and 10 MPa (and 14 wt.% at 100 K and 20 MPa) for Li-doped, optimally configured CNT assemblies [125]. DFT calculations also predict high capacities for Au-doped CNTs (e.g., 5.05 wt.% and 298.62 g L^{-1}) under idealised geometries [78]. Importantly, these values should be treated as computational upper-bound targets (computational-only), because they rely on dopant dispersion and defect-free, unblocked CNT packing that is difficult to realise experimentally; dopant clustering, tube blocking, and structural defects are likely to reduce and destabilise the achievable reversible

View Article Online
DOI: 10.1039/D5SE01539A

uptake at room temperature.

These diverse synthesis routes and post-treatment processes often yield contrasting results, even for seemingly similar materials, underscoring the importance of reproducibility and standardized evaluation protocols. Minor variations in metal dispersion, pore accessibility, or defect concentration can dramatically alter adsorption behavior. Consequently, reports of unusually high ambient-temperature H_2 uptake by carbon materials must be interpreted cautiously and validated through repeated measurements under well-defined equilibrium conditions to distinguish true physisorption from measurement artifacts or chemisorption contributions.

3.2. Metal-Organic Frameworks (MOFs)

Metal-Organic Frameworks (MOFs) are a unique class of porous materials that offer remarkable stability and flexibility[127]. Composed of metal ions or clusters coordinated with organic ligands, MOFs feature tunable pore sizes and functionalities, making them excellent for gas adsorption and separation [128]. To enhance H_2 uptake at ambient conditions, key factors include improving interactions between MOF surfaces and H_2 molecules, incorporating energetic sites within the pores, and ensuring accessible open metal sites[129,130].

The following content discusses various MOFs studied for hydrogen storage at ambient temperatures, highlighting their adsorption mechanisms.

As illustrated in **Figure 8a**, the BET surface area of this MOF series scales approximately linearly with the micropore volume ($S_{\mathrm{BET}} \approx 2455\, V_{\mathrm{pore}}$), indicating that increases in microporosity translate directly into additional accessible surface. **Figure 8b** shows that the total hydrogen adsorption at 298 K and 100 bar also follows an approximate linear trend with BET area, with a best-fit relation $H_2^{\mathrm{tot}}(\mathrm{wt\%}) \approx 0.5 \times S_{\mathrm{BET}}/1000$. Although this correlation

View Article Online
DOI: 10.1039/D5SE01539A

may not be a universal law in the same sense as the Chahine rule at 77 K (1wt%~500m^2/g), it demonstrates that such studies have established a clear, though approximate, proportionality between surface area and high-pressure ambient-temperature capacity, underscoring that BET area (and thus micropore volume) remains an important descriptor even at room temperature.

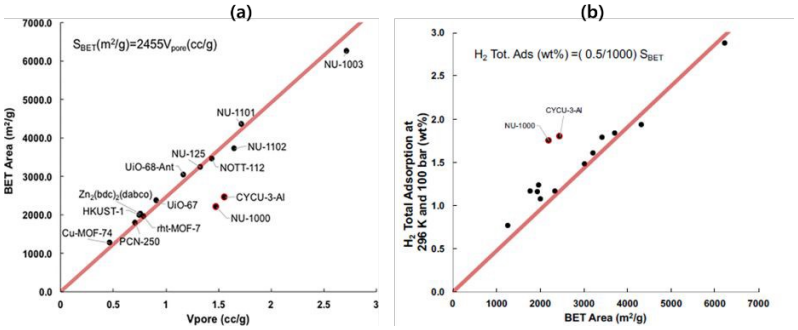

Fig. 8. Comparison of (a) BET surface area and pore volume, and (b) total H_2 uptake with respect to the BET surface area[52]. (Reproduced from ref. 52 with permission from The American Chemical Society, copyright 2018)

A comparative analysis of representative MOFs, including MOF-5, HKUST-1, NU-1000, MIL-101, and DUT-6, reveals distinct structural and adsorption characteristics under ambient and moderate pressure conditions (≤200 bar). MOF-5, with a large surface area (3,000–3,800 $m^2\ g^{-1}$) and uniform micropores (~1.2–1.5 nm), exhibits moderate hydrogen uptake (~0.3 wt% at 298 K and 100 bar), primarily driven by weak van der Waals interactions [131]. A beryllium-based MOF, $Be_{12}(OH)_{12}$(1,3,5-benzenetribenzoate)$_4$, with a very high surface area (4,030 $m^2\ g^{-1}$) demonstrates an exceptional H_2 capacity of 2.3 wt% (11 g L^{-1}) at 298 K due to optimal pore size and structure [132]. Similarly, two Co-based MOFs, [Co_3(bdc)$_3$(dabco)] and [Co_3(ndc)$_3$(dabco)], show that structural tuning through ligand modification can substantially affect adsorption; the latter achieves 0.89 wt% at 17.2 bar and 298 K [133]. A Cu-based MOF, Cu(hfipbb)(H_2hfipbb)$_{0.5}$, with interpenetrated paddle-wheel units and 1D microporous channels (~3.5–5.1 Å), exhibits notable H_2 uptake of 1 wt% at

View Article Online
DOI: 10.1039/D5SE01539A

48 atm and 25 °C with a high volumetric density (0.0147 g H_2 cm^{-3}) [134]. Furthermore, a Zn-based microporous MOF, $[Zn_7O_2(pda)_5(H_2O)_2]\cdot 5DMF\cdot 4EtOH\cdot 6H_2O$, containing a heptanuclear metal cluster, stores 1.01 wt% (112.4 mL g^{-1}) at 71.4 bar and maintains reversibility over multiple cycles [135]. Another concept of interpenetrated MOFs with optimized microporous structures has also been proposed as a promising material for volumetric hydrogen storage capacity. The interpenetrating networks can enhance host–guest interactions through an entrapment mechanism, where H_2 molecules are surrounded by multiple aromatic rings, leading to improved adsorption [136]. Lin and coworkers synthesized two highly interpenetrated Zn-based MOFs, $[Zn_4(\mu_4\text{-}O)(L_1)_3(dmf)_2]\cdot 4DMF\cdot 3CH_3OH\cdot 2H_2O$ and $[Zn_4(\mu_4\text{-}O)(L_2)_3]\cdot 5DMF\cdot 5C_2H_5OH\cdot H_2O$, showing H_2 uptakes of 1.12 wt% and 0.98 wt% at 48 bar and room temperature, respectively. Despite their relatively low surface areas, these high capacities are attributed to the interpenetrated frameworks[137]. Similarly, a Cd-based MOF, $[Cd_3(bpdc)_3(DMF)]\cdot 5DMF\cdot 18H_2O$ (JUC-48), with large 1D tubular channels, demonstrates 1.1 wt% H_2 uptake at 100 bar and room temperature [138]. Cu-based MOFs such as PCN-68 and PCN-610, constructed using dendritic hexa-carboxylate ligands, also show notable adsorption behavior; PCN-68 achieves 10.1 mg g^{-1} H_2 uptake at 90 bar and 298 K due to its higher porosity (82.9%) and pore volume compared with PCN-61 and PCN-66 [139].

It has been well documented in the literature that incorporating energetic sites via the implementation of organometallic complexes, crown ethers, and some ammonium borane species can increase H_2 storage capacity at RT [140,141]. For example, a LiCrw-complex was incorporated in Cr-MIL-101 (MIL stands for *Materials from Institut Lavoisier*), Fe-MIL-100, and Ni-MOF-74 by *Gisela Orcajo and coworkers,* resulting in around 59% and 23% enhancement in the uptake of H_2 in the case of crown ether doped MIL-100 and MIL-101, respectively, at RT. In Li-doped MIL-100 and MIL-101, the enhancements were around 98%

View Article Online
DOI: 10.1039/D5SE01539A

and 67%, respectively (**Table 3**)[142]. Similarly, the inclusion of $(TBA)_2Mo_6Br_8F_6$ (TBA = tetrabutylammonium) containing $[Mo_6Br_8F_6]^{2-}$ cluster units within the pores of the mesoporous chromium carboxylate MIL-101 has also been investigated, and found that at RT and 8 MPa, the H_2 storage capacity of the MIL-101-$Mo_6Br_8F_6$ is over twice that of MIL-101[143].

Table 3. Comparison of volumetric H_2 adsorption capacity by modified MOFs at 298 K and 170 bar[142].

Material	SBET (m2/g)	V_p NL-DFT (cm^3/g)	Excess volumetric H_2 adsorption capacity (g/L) at 298 K and 170 bar	Total volumetric H_2 adsorption capacity (g/L) at 298 K and 170 bar
Cr-MIL-101	2589	1.15	2.68	10.89
Crw@Cr-MIL-101	2285	0.94	4.26	11.52
LiCrw@Cr-MIL-101	2159	0.89	5.35	12.27
Fe-MIL-100	1350	0.83	3.10	10.82
Crw@Fe-MIL-100	822	0.44	3.81	10.54
LiCrw@Fe-MIL-100	742	0.39	5.17	11.21
Ni-MOF-74	1286	0.48	5.71	10.43
Crw@Ni-MOF-74	638	0.27	5.17	9.22
LiCrw@Ni-MOF-74	595	0.23	4.09	7.39

Furthermore, the introduction of open metal sites (OMS) and the formation of mixed-metal sites in MOFs could also enhance H_2 storage [144]. The OMS involves the Kubas interaction by which the bond length of H_2 molecules slightly increases[145]. The $V_2Cl_{2.8}$(btdd) (H_2btdd, bis(1H-1,2,3-triazolo[4,5-b],[4′,5′-i])dibenzo[1,4]dioxin) MOF, having the unsaturated V(II) site that can adopt H_2 efficiently. The study has been well explained using powder neutron X-ray diffraction and variable-temperature IR spectroscopy. The resulting binding enthalpy was -21 kJ/mol, which is within the range of H_2 storage at ambient temperature[146]. Having open metal sites, four MOFs; M_2(m-dobdc) and M_2(dobdc) (where m-dobdc^{4-} = 4,6-dioxido-1,3-benzenedicarboxylate, dobdc^{4-} = 1,4-dioxido-1,3-benzenedicarboxylate) have been synthesized using Co and Ni that showed high H_2 storage capacity at near ambient temperature (**Fig. 9**). Out of these four, the Ni_2(m-dobdc) showed top performance to store the H_2 at ambient temperature with high usable capacity. A usable volumetric capacity of 11.0 g/L was observed at 25 °C between 100 and 5 bar, while it was 23.0 g/L between -75 to 25 °C[147].

View Article Online
DOI: 10.1039/D5SE01539A

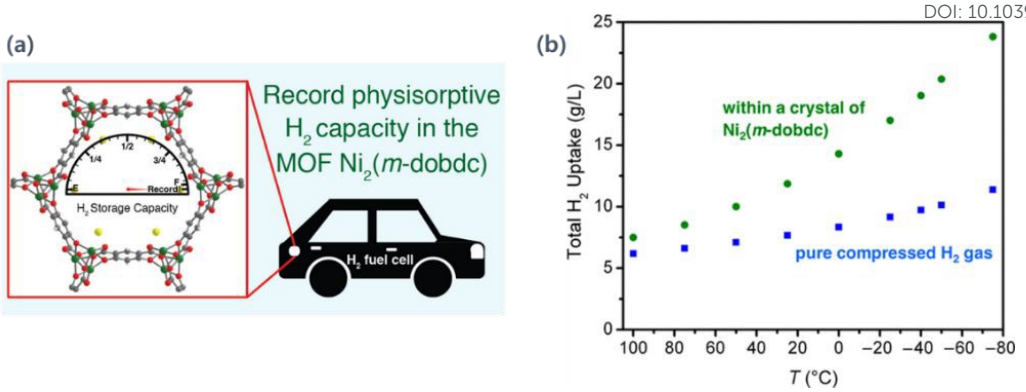

Fig. 9. (a) Schematic illustration of the physisorptive H_2 capacity in Ni_2(m-dobdc) and (b) comparison of total volumetric capacities and pure compressed H_2 of Ni_2(m-dobdc) at 100 bar[147]. (Reproduced from ref. 147 with permission from The American Chemical Society, copyright 2018).

Moreover, $[Mn(DMF)_6]_3[(Mn_4Cl)_3(BTT)_8(H_2O)_{12}]_2 \cdot 42DMF \cdot 11H_2O \cdot 20CH_3OH$ MOF, having an unsaturated metal site, has been used, which showed 0.94 wt% of H_2 storage at 90 bar and RT[148]. Similarly, the Cu(I) site in the MOFs also provides a strong, unsaturated (open) metal site that facilitates the storage of H_2 at RT with high efficiency. In this regard a series of Cu^I-MFU-4l-based MOF ($Cu_{2.7}M_{2.3}X_{1.3}(btdd)_3$) (M = Mn, Cd; X = Cl, I; H_2btdd = bis(1H-1,2,3-triazolo-[4,5-b],[4′,5′-i])dibenzo[1,4]dioxin; Cu^IM-MFU-4*l*) have been reported which has been synthesized by post-synthetic modification of $M_5X_4(btdd)_3$ (M = Mn, Cd; X = CH_3CO_2, I). This strategy modulates the H_2 adsorption enthalpy at the Cu(I) sites by adjusting the ionic radius of the central metal ion in the pentanuclear cluster node. Based on this, the storage capacity of H_2 was observed as follows at 298 K and 5-100 bar: 1.5 wt% (ZnCl-MFU-4*l*), 1.6 wt% (Cu^IZn-MFU-4*l*), 1.4 wt% (Cu^IMn-MFU-4*l*), and 1.4 wt% (Cu^ICd-MFU-4*l*). These values are higher than those of many other MOFs with open metal sites[149].

The hydrogen spillover process in MOFs generally involves three steps: dissociative activation of H_2 on a metal catalyst, migration of atomic hydrogen through a support matrix, and subsequent adsorption within the MOF framework [122,150]. Early studies suggested that this mechanism enhances hydrogen storage at ambient temperatures through combined

View Article Online
DOI: 10.1039/D5SE01539A

physisorption and chemisorption, with reported improvements in MOFs such as MOF-5, IRMOF-8, and MIL-100 after incorporating Pt/AC or Li-decorated components (**Fig. 10**) [86,151][150][152][153][154]. However, subsequent investigations have shown that while hydrogen spillover can occur as a surface phenomenon, it does not contribute significantly to reversible hydrogen storage. Many experimental and theoretical studies have failed to reproduce earlier claims of large spillover-induced enhancements, revealing that the mechanism likely leads to irreversible chemisorption rather than usable hydrogen capacity. As in carbon-based materials, hydrogen spillover is now considered an ineffective mechanism for practical hydrogen storage under ambient conditions[155–158].

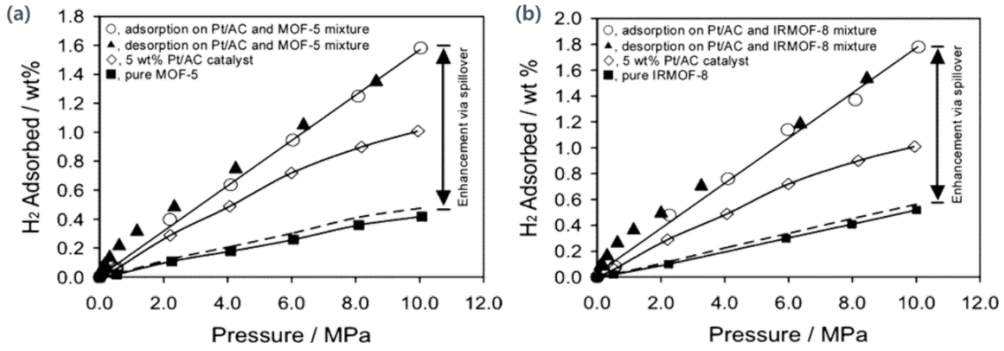

Fig. 10. Comparison of H_2 storage isotherms showing enhancement via the spillover effect for (a) pure MOF-5 and modified with Pt/Ac and (b) IRMOF-8 modified with Pt/Ac at 298 K[150]. (Reproduced from ref. 150 with permission from The American Chemical Society, copyright 2006).

Table 4. List of selected MOFs used for H_2 storage at RT.

Sr. No	Materials	BET Surface area (m^2/g)	Pore volume (cm^3/g)	H_2 storage capacity	P (bar)	Mech.	Ref.
1	$V_2Cl_{2.8}$(btdd)	1920 3350*	1.12	1.64 wt%, 0.26 mmol/g	1.2	OMS	[146]
2	Ni_2(m-dobdc)	1321	0.56	0.98 wt%, 11.9 g/L	100	OMS	[147]
3	Ni50Co-IRMOF-74	1985	0.86	0.39 wt%, 3.1 g/L	100	OMS/MMS	[129]
4	$Mn_3[(Mn_4Cl)_3(BTT)_8]_2$ (Mn-BTT)	2100	0.795	0.94 wt%	90	OMS	[148]
5	$Zn_5Cl_4(btdd)_3$ (ZnCl-MFU-4l)	3470 3880*	1.38	1.5 wt%, 8.5 g/L	5 to 100	OMS	[149]
6	$Cu^I_{2.2}Zn_{2.8}Cl_{1.8}(btdd)_3$ (Cu^IZn-MFU-4l)	3660 4080*	1.45 / 1.59	1.6 wt%, 8.2 g/L	5 to 100	OMS	[149]
7	$Cu^I_{2.7}Mn_{2.3}Cl_{1.3}(btdd)_3$ (Cu^IMn-MFU-4l)	3000, 3340*	1.19 / 1.76	1.4 wt%, 6.8 g/L	5 to 100	OMS	[149]
8	$Cu^I_{2.7}Cd_{2.3}I_{1.3}(btdd)_3$ (Cu^ICd-MFU-4l)	2930, 3280*	1.18 / 1.40	1.4 wt%, 8.5 g/L	5 to 100	OMS	[149]
9	Ni_2(dondc)	1942	1.16	10.74 g L−1	100	OMS	[144]
10	MOF-5 Pt/Ac	1021	0.39	1 wt%	100	SPO	[150]
11	Li-C60@Li-IRMOF-10	-	-	6.3 wt%	100 (243 K)	SPO	[154]
12	IRMOF-8	-	-	0.5 wt%	100	SPO	[152]
13	IRMOF-8 Pt/Ac	548	0.48	1.5 wt%	100	SPO	[152]
14	IRMOF-8 Pt/Ac (bridge enhancement)	466	0.43	4.0 wt%	100	SPO	[152]
15	MIL-100	1960	0.980	0.25 wt%	31	SPO	[153]

View Article Online
DOI: 10.1039/D5SE01539A

		2691*					
16	Pt/Ac-MIL-100	1552	0.889	0.41 wt%	31	SPO	[153]
17	$Be_{12}(OH)_{12}(BTB)_4$	4030 4400*	-	2.3 wt%, 11g/L	95	Optimal pore size and surface area	[132]
18	$Co_3(ndc)_3(dabco)$	1502 2293*	0.82	0.89 wt%, 10.8 g/L	17.231	Optimal pore size and surface area	[133]
19	$Cu(hfipbb)(H_2hfipbb)_{0.5}$	-	-	1 wt%, 14.7 g/L	48	Optimal pore size and surface area	[134]
20	$Zn_4O(dcdEt)_3$	502	0.2	1.12 wt%	48	Interpenetrated Framework	[137]
21	$Zn_4O(dcbBn)_3$	396	0.13	0.98 wt%	48	Interpenetrated Framework	[137]
22	$Zn_7O_2(pda)_5(H_2O)_2$		0.17	1.01 wt%	71.43	Optimal pore size and surface area	[135]
23	$Cd_3(bpdc)_3$ (JUC-48)	880*	0.19	1.1 wt%	100	1D nanotube-like channels	[138]
24	$Cu_3(ptei)$ (PCN-68)	5109 6033*		1.01 wt%, 4.1 g/L	90	Optimal pore size and surface area	[139]
25	Co(HBTC)(4,4' -bipy)·3DMF	887	0.54	0.96 wt%	72	Optimal pore size and surface area	[159]
26	Ni(HBTC)(4,4' -bipy)·3DMF	1590	0.81cm3/g	1.2 wt%	72	Optimal pore size and surface area	[159]
27	UIO-66 (In different forms and activation conditions)	180-1413	0.12-0.61	0.7-0.8 wt%	100	Porosity and optimal pore size	[53]
28	MOF-519	2400	0.94	0.97 wt%	100	Ligand and metal site	[160]
29	MOF-520	3290	1.28	1.27 wt%	100	Ligand and metal site	[160]
30	LiCrw@Cr-MIL-101	2159	0.89	0.7 wt%, 12.27 g/L	170	ESI	[142]
31	Fe-MIL-100	742	0.83 cm3/g	0.5 wt%, 10.82 g/L	170 bar	ESI	[142]
32	MIL-101-$Mo_6Br_8F_6$	-		0.4 wt%	8 MPa	ESI	[143]
33	Ti-Decorated Mg-MOF-74	1206		2 wt% 1.29 Wt%	1 bar 1 bar	DFT	[161]

*= Langmuir surface area, OMS: open metal site, SPO: spillover mechanism, MMS: mixed metal site, ESI: energetic site incorporation

View Article Online
DOI: 10.1039/D5SE01539A

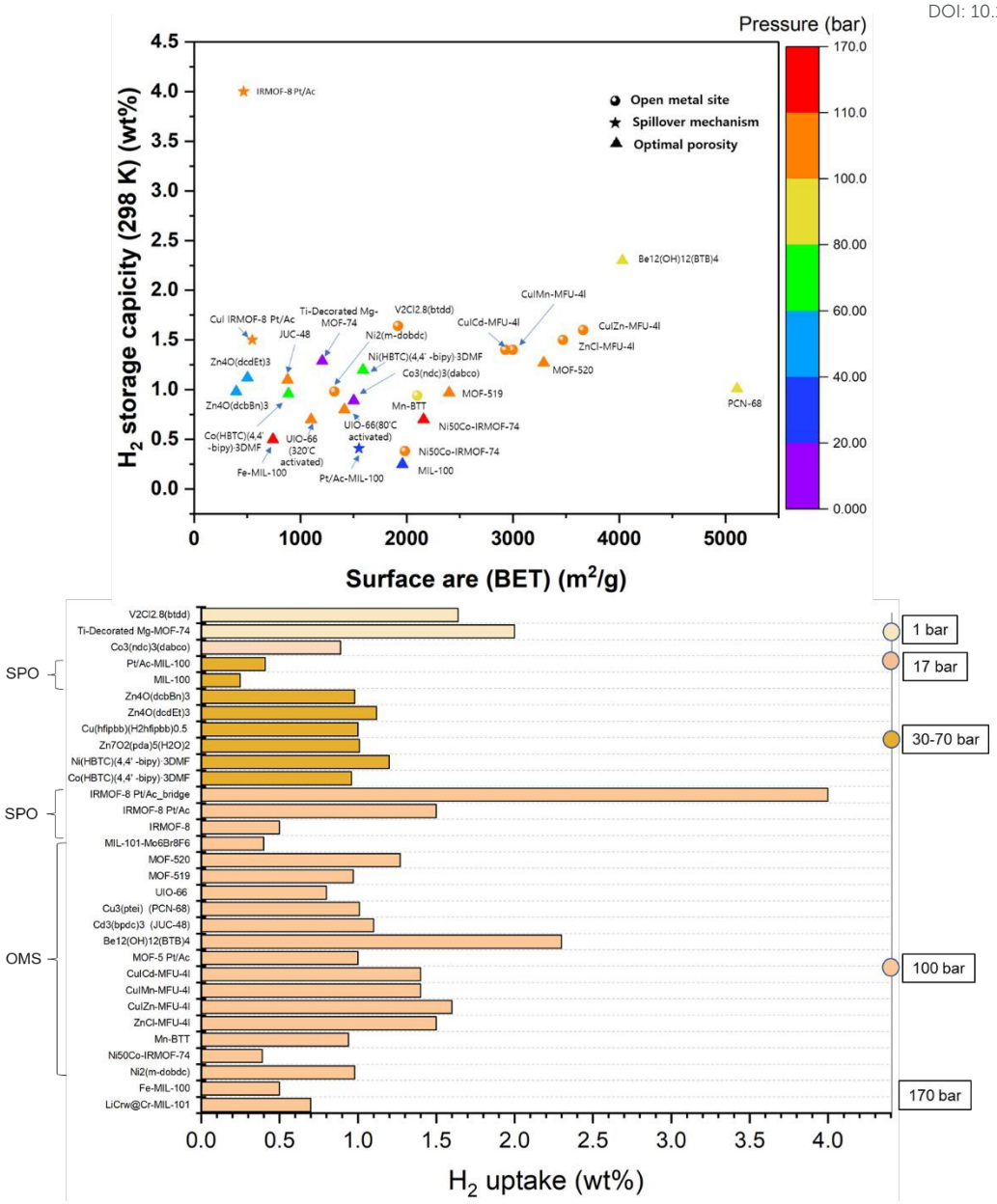

Fig. 11. Comparison of the H_2 storage capacities of different types of MOFs concerning surface area and pressure at RT.

We summarize H_2 storage at RT in this section, using examples of different MOFs and their mechanisms. Comparing H_2 storage capacity with surface area and pore volume reveals that high surface area does not always guarantee high storage capacity at RT (Fig. 11). For instance, PCN-68 and $Be_{12}(OH)_{12}(BTB)_4$ are both utilized for hydrogen storage at pressures between 80 and 100 bar and at room temperature. Notably, $Be_{12}(OH)_{12}(BTB)_4$, which has a specific surface

View Article Online
DOI: 10.1039/D5SE01539A

area of 4030 m²/g, demonstrates a superior storage capacity of 2.3 wt% at 95% compared to PCN-68, which has a storage capacity of 1.01 wt% at 90%, despite PCN-68 having a higher surface area of 5109 m²/g. Storage capacity is also influenced by factors such as pore size and the presence of open metal sites. A similar trend has also been observed in the case of MOFs with open metal sites, where materials with high surface area could possess high storage of H_2, but other factors, such as optimal pore size and the presence of certain functionalities, also affect the storage (**Fig. 11**). Most of the MOFs that have been used for H_2 storage at RT are summarized in **Table 4**.

MIL-100 exhibited a hydrogen uptake of 0.25 wt%, which increased to 0.41 wt% after Pt/AC-assisted spillover. The theoretically predicted hydrogen uptake[162] and adsorption enthalpy at room temperature are generally higher than the corresponding experimental values. For instance, while MIL-100 exhibits an experimental hydrogen uptake of approximately 0.25 wt%, theoretical simulations predict an enhanced uptake of up to ~0.8 wt% at 100 bar and room temperature. Similarly, IRMOF-8 showed an uptake of 0.5 wt%, which was enhanced to 1.5 wt% for IRMOF-8-Pt/AC and further increased to 4 wt% for Pt/AC-bridged IRMOF-8. One should note that these studies *reported* enhanced RT uptake after Pt/AC-assisted "spillover" treatments (e.g., MOF-5 Pt/AC, IRMOF-8 Pt/AC, and Pt/AC-bridged IRMOF-8). However, the spillover concept has undergone substantial re-evaluation over time: multiple follow-up studies have questioned the magnitude, reversibility, and reproducibility of spillover-driven gains under ambient conditions, suggesting that any apparent enhancement may include surface chemisorption or measurement/analysis artifacts rather than a robust increase in reversible physisorption capacity. Consequently, exceptionally high SPO-labelled values in Table 4 (e.g., 4.0 wt% for Pt/AC-bridged IRMOF-8, and 6.3 wt% reported for Li-C60@Li-IRMOF-10 at 243 K) should be considered provisional unless supported by cycling stability, independent method

View Article Online
DOI: 10.1039/D5SE01539A

cross-checks, and unambiguous excess-uptake reporting.

(Reproducibility challenges) MOFs are highly tunable materials with exceptional surface areas and porosities, making them promising candidates for physisorption-based hydrogen storage. However, their reproducibility is often hindered by the extreme sensitivity of their synthesis process to small variations in experimental conditions such as solvent type, synthesis temperature, pH, and reaction time. Even minor deviations in these parameters can lead to differences in crystal morphology, particle size distribution, and defect concentration, all of which significantly affect adsorption performance. For example, variations in solvothermal synthesis temperature alter the coordination environment of metal nodes or the orientation of linkers, resulting in frameworks with slightly different pore volumes or surface chemistries. Consequently, reproducing identical MOF samples across different laboratories remains a significant challenge[163–167].

Another key factor affecting reproducibility is the moisture sensitivity of many MOFs. Exposure to ambient humidity during synthesis, activation, or storage can lead to partial hydrolysis of metal–ligand bonds or blockage of pore sites by adsorbed water molecules. Hydrophilic MOFs such as HKUST-1 or MOF-5 are particularly prone to degradation upon contact with moisture, leading to a reduction in crystallinity and hydrogen uptake capacity[167]. Even small amounts of residual water can alter adsorption isotherms by competing with hydrogen for active sites or changing the surface polarity. Therefore, maintaining rigorous control over environmental conditions, such as performing synthesis and handling in inert atmospheres and storing samples in desiccators, is crucial for ensuring reproducible adsorption behavior[168,169].

Structural instability further complicates reproducibility in MOF-based hydrogen storage studies. Some frameworks undergo partial collapse or amorphization during solvent removal,

View Article Online
DOI: 10.1039/D5SE01539A

thermal activation, or repeated adsorption–desorption cycles, especially those with flexible linkers or weak coordination bonds. This structural degradation leads to significant variations in pore accessibility and surface area between measurements. Additionally, differences in activation temperature or duration can exacerbate instability, resulting in inconsistent hydrogen uptake even for nominally identical samples[170,171]. To overcome these challenges, researchers are focusing on developing more robust MOFs with enhanced hydrothermal stability and on establishing standardized synthesis and activation protocols to ensure that structural integrity and, thus, adsorption performance remain consistent across studies.

3.3. Covalent Organic Frameworks (COFs)

COFs, which are porous materials formed by the condensation of two organic moieties, showed excellent efficiency in storing H_2[172]. However, only a few reports show storage at ambient temperature. Here are examples of COFs used for H_2 storage at RT. COFs provide high surface area and functionalities that can accommodate H_2 molecules with weak interactions. A few studies in the literature report high H_2 storage efficiency at RT. For example, a 2D COF named H2P-COF, which has a tetrapyridine-bridged structure, showed 5 wt% volumetric uptakes of H_2 at 298 K and 100 bar, which is higher than many 2D materials. The storage is primarily due to the high free volume of the COF, which can accommodate a large amount of H_2[173]. Similarly, four tetraphenyl silsesquioxane-based 3D COFs named sil-COF-1-4 have been synthesized and investigated for H_2 storage at RT. Computational results revealed that these materials possess high surface area and porosity, with one COF exhibiting 5.50 wt% H_2 storage at room temperature[174].

Many reports have shown that H_2 storage performance can be boosted in these materials through doping or other methods [175]. One such report is the enhancement of the H_2 storage capacity of COF-108 through carbon nanotube insertion, lithium doping, and boron

View Article Online
DOI: 10.1039/D5SE01539A

substitution. Li-doped and B-substituted COF-108 observed a computational value of 5.08 wt% H_2 uptake at 298 K and 100 bar[176]. Similarly, using a multiscale theoretical method, another study predicts that COF-105 and COF-108 have superior H_2 storage capacities. At RT (298 K) and 100 bar, Li-doped COF-105 and COF-108 achieve storage capacities of 6.84 and 6.73 wt%, respectively, making them the most promising candidates for H_2 storage[177].

Despite the structural tunability of covalent organic frameworks (COFs), robust experimental validation of room-temperature H_2 physisorption in COFs remains limited, and the highest capacities frequently cited for COFs are dominated by computational projections rather than reproducible experimental datasets. Accordingly, we discuss COFs by explicitly separating (i) computational upper-bound targets (DFT/GCMC) from (ii) experimentally reported trends, emphasizing the significant simulation–experiment gap.

A number of studies have proposed that COF performance at ambient temperature could be increased by rational topological design and functionalization. For example, four novel three-dimensional COFs were designed by replacing the phenylene units in COF-102 with extended aromatic building blocks while preserving the original topology. DFT optimization followed by GCMC simulations suggested that one candidate could reach ~6.5 wt% at 300 K and 100 bar [178,179]. Using a similar simulation workflow, an adamantane-based COF (adm-COF; 1,3,5,7-tetraphenyladamantane) with a simulated surface area of 5967–6709 $m^2\ g^{-1}$ was predicted to store 5.81 wt% H_2 at room temperature and 100 bar [182]. These results should be interpreted as computational-only upper-bound targets, because they typically assume ideal crystallinity, defect-free stacking/porosity, and adsorption-site accessibility that are difficult to realize consistently in experimental COF solids.

View Article Online
DOI: 10.1039/D5SE01539A

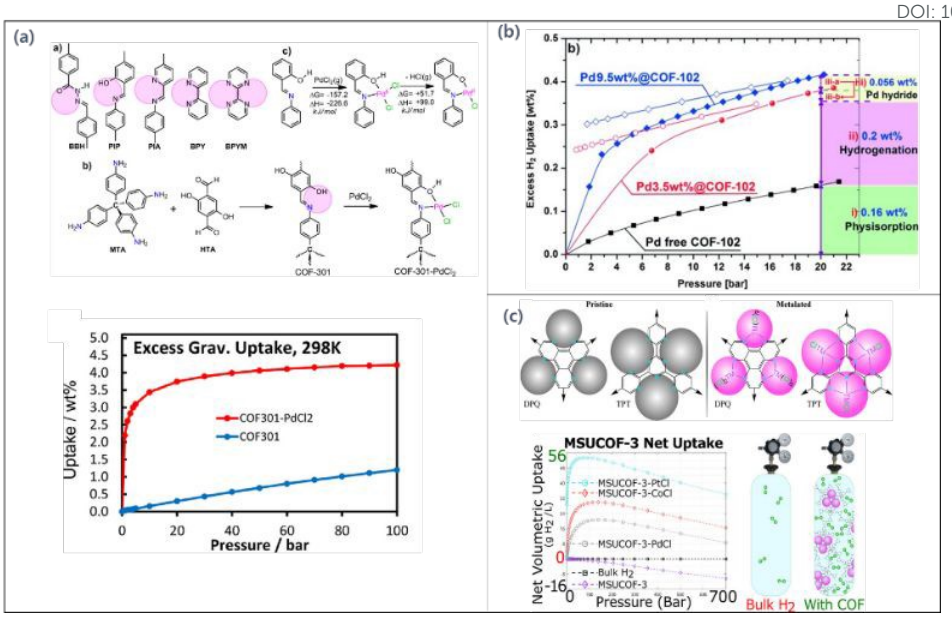

Fig. 12. (a) Representative COF ligand structures and reported room-temperature hydrogen uptake (experimental literature)[180, 185] (Reproduced from ref. 180 with permission from The American Chemical Society, copyright 2012), (b) Reported room-temperature uptake enhancement in Pd nanoparticle–COF composites (COF-102 example)[158] (Reproduced from ref. 158 with permission from The American Chemical Society, copyright 2023) and (c) Schematic/representative report of spillover-like concepts discussed for COFs at 298 K [181] (Reproduced from ref. 181 with permission from Wiley, copyright 2012).(Panels (b–c) are included to illustrate proposed/claimed enhancement strategies; independent verification and standardized testing remain important for assessing reproducibility.).

Computational work also suggests that introducing stronger binding motifs can increase adsorption enthalpy (Qst) and thereby raise room-temperature uptake. Quantum-mechanical calculations predicted that $PdCl_2$-incorporated COF-301 could store up to 60 g L^{-1} (4.2 wt%) of hydrogen at 100 bar, exceeding the DOE 2015 volumetric target by ~1.5×, despite reductions in surface area and pore volume. The proposed origin is strong Pd–H_2 interactions that increase Qst from ~6 to ~23 kJ mol^{-1} [183]. Importantly, however, experimental realization has not yet been achieved, likely due to limited diffusion/penetration of $PdCl_2$ into COF-301 pores [183]. This case illustrates a central challenge for COFs: simulated performance gains often rely on

View Article Online
DOI: 10.1039/D5SE01539A

uniform, pore-accessible incorporation of dopants, which is experimentally non-trivial and can introduce pore blocking, heterogeneity, and poor batch-to-batch reproducibility.

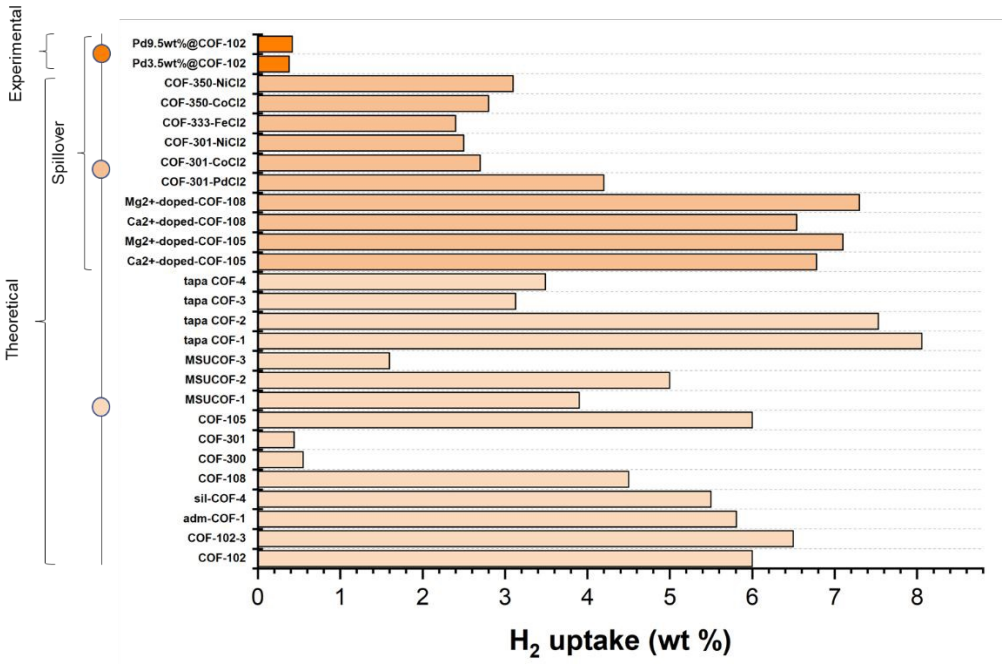

Fig. 13. Summary of COF hydrogen storage at room temperature, separating experimental results from computational-only (DFT/GCMC) predictions and highlighting entries that require further independent verification..

In parallel, several studies have reported or proposed that metal nanoparticle composites with COFs can enhance apparent room-temperature storage via a spillover-like mechanism, conceptually similar to strategies explored in MOFs [184]. For instance, Pd nanoparticle incorporation into COF-102 has been reported as a route to increase room-temperature uptake (Fig. 12b) [158], and spillover-enabled enhancement has also been discussed in the COF context (Fig. 12c) [181]. Figure 13 presents a comparison of the hydrogen storage capacities of COFs under room-temperature conditions.

Although COF materials are often highlighted as promising candidates for hydrogen storage, their reported high storage capacities are currently derived only from computational simulations rather than experimentally validated data. This indicates that further synthesis and

View Article Online
DOI: 10.1039/D5SE01539A

measurement under practical conditions are required to confirm their actual performance.

4. Critical Factors Affecting Measurement Reproducibility

4.1. Materials-oriented reproducibility factors

Consistency in Sample Preparation

Consistency in sample preparation is critical for reproducible hydrogen adsorption measurements, as variations in powder homogeneity, compaction density, particle size, and morphology can significantly influence gas accessibility and adsorption kinetics. Inhomogeneous powders or irregular particle sizes can lead to non-uniform packing in measurement cells, creating regions of restricted gas diffusion and uneven exposure of adsorption sites[186–188]. Similarly, compaction density affects pore accessibility, as overly dense packing may block micropores, while loosely packed samples may result in poor thermal and pressure equilibration. Controlling these parameters and carefully documenting sample preparation methods ensures that adsorption measurements accurately reflect the intrinsic properties of the material rather than artifacts of sample handling[189,190].

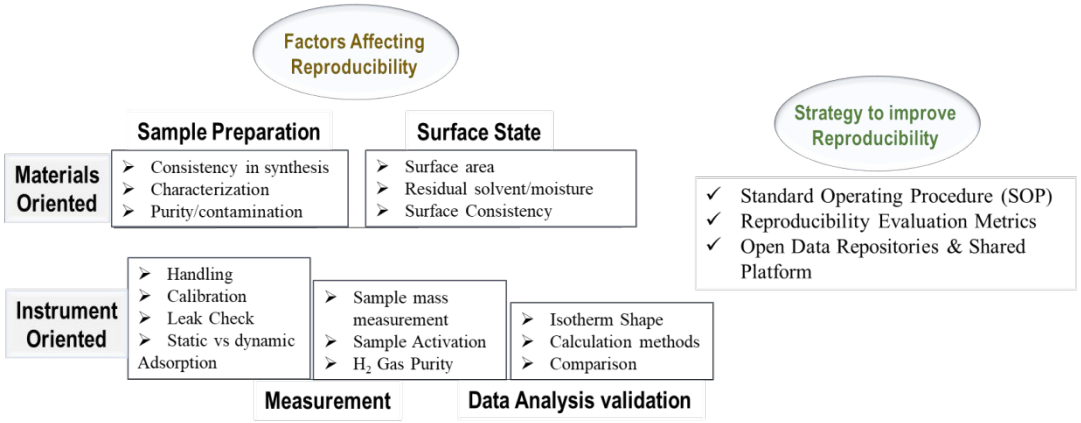

Fig. 14. Common factors affecting and strategies to improve the reproducibility.

The purity of hydrogen gas used in adsorption experiments is another crucial factor affecting reproducibility. Even trace amounts of impurities such as nitrogen, oxygen, or water vapor can compete with hydrogen for adsorption sites, alter surface interactions, or chemically react with

View Article Online
DOI: 10.1039/D5SE01539A

sensitive materials. For example, water can strongly adsorb onto polar sites within metal–organic frameworks (MOFs), reducing effective hydrogen uptake, while oxygen contamination may oxidize metal centers, altering the material's structural and chemical properties. Using high-purity hydrogen (>99.999%) and incorporating purification steps such as gas drying, oxygen scrubbing, or in-line molecular sieves can minimize these effects. Careful monitoring and reporting of gas purity, along with proper system leak testing, are essential to ensure that adsorption data are both accurate and reproducible across different laboratories[191–193].

Variability in Surface Area and Structural Characterization

Porosimetry techniques, including gas adsorption isotherm analysis, and density functional theory (DFT) modeling, often produce variable pore size distributions depending on measurement conditions and data interpretation methods. In the context of MOFs and other microporous materials, the selection of adsorbate gas (N_2, Ar, or CO_2) and temperature can lead to considerable discrepancies, particularly when differentiating between micro- and mesopores[194]. For instance, argon adsorption at 87 K may reveal additional pore features that nitrogen adsorption at 77 K cannot capture due to diffusion limitations. Moreover, differences in data reduction methods, such as Barrett–Joyner–Halenda (BJH), Horvath–Kawazoe (HK), or nonlocal DFT (NLDFT), can yield inconsistent pore-size profiles even for the same isotherm. Instrumental factors, including sample mass accuracy, equilibration time, and vacuum efficiency, further compound these reproducibility challenges[195,196]. To achieve consistent characterization, researchers are encouraged to adopt harmonized data analysis protocols and report both experimental parameters and fitting models in detail.

Consistency of Surface State

(*Contaminants and Variability in Pretreatment*) To achieve reproducibility in hydrogen adsorption measurements, several factors must be considered (**Fig. 12**). The surface state of

View Article Online
DOI: 10.1039/D5SE01539A

porous materials plays a decisive role in determining the reproducibility of adsorption-based hydrogen storage measurements. Inconsistencies in sample preparation, activation, and measurement directly affect the availability of adsorption sites and, consequently, the measured hydrogen uptake [197]. Surface contaminants originating from synthesis precursors, environmental exposure, or incomplete purification can further compromise reproducibility by modifying the chemical environment of adsorption sites. These contaminants may alter surface polarity, block pore entrances, or catalyze undesired reactions that affect hydrogen interaction[198,199]. For instance, organic residues or metal oxide by-products can reduce the effective BET surface area, resulting in lower and more inconsistent adsorption capacities. To ensure accuracy, characterization methods such as FTIR, XPS, and elemental analysis should be employed to confirm surface cleanliness after activation. Ultimately, establishing standardized pretreatment and handling protocols, along with thorough surface characterization, is essential to achieve reproducible, comparable hydrogen storage measurements across different laboratories and research groups.

Pretreatment steps such as solvent exchange, vacuum drying, and thermal activation are intended to remove guest molecules, solvents, or impurities from the pore structure, thereby exposing the active adsorption sites[200]. Inconsistent pretreatment procedures can lead to significant deviations in measured capacities, even for identical materials. Vacuum drying and thermal treatment are among the most influential factors governing the surface state of MOFs and other porous adsorbents. An incomplete activation process may leave residual solvent molecules within the pores, blocking the internal surface area and reducing adsorption capacity. Conversely, excessively high activation temperatures or prolonged heating times can damage the framework, particularly in thermally sensitive MOFs, leading to partial collapse of the pore network. Therefore, identifying optimal activation parameters for each material type is crucial.

View Article Online
DOI: 10.1039/D5SE01539A

Researchers often employ thermogravimetric analysis or in situ gas adsorption techniques to monitor desolvation and ensure that the material reaches a reproducible and stable activated state before hydrogen measurement[201].

(*Residual moisture*) Residual moisture is another major factor that can significantly alter adsorption performance and measurement reproducibility. Water molecules are highly polar and can strongly adsorb onto metal centers or within pore cavities, displacing hydrogen and reducing the number of available adsorption sites. Even trace amounts of moisture introduced during sample handling, storage, or measurement can lead to inconsistent results between laboratories. To mitigate this, samples are often handled in inert atmospheres, such as glove boxes filled with dry nitrogen or argon, and stored in desiccators before testing. Additionally, pre-drying of adsorbates and the use of moisture traps in the measurement system can further minimize variability caused by water adsorption[202].

The structural stability of MOFs under humid conditions is a critical concern for their practical use in gas storage, as eliminating water vapor from industrial gas streams is often challenging. Unfortunately, several MOFs, including MOF-5, MOF-177, and SNU-5, exhibit partial structural degradation upon exposure to air, as evidenced by changes in their PXRD patterns. This deterioration leads to a pronounced reduction in their gas adsorption capacities, highlighting the need for moisture-resistant framework designs[203–205].

4.2. Instrumental-oriented reproducibility factors

Static vs. dynamic adsorption systems

The type of adsorption measurement system, static (volumetric) or dynamic (gravimetric or flow-based), can introduce notable variations in recorded hydrogen uptake values. Static systems rely on pressure–volume–temperature (PVT) relationships to calculate the adsorbed quantity, while dynamic systems measure mass changes or gas flow directly. Each method has

View Article Online
DOI: 10.1039/D5SE01539A

inherent strengths and limitations: volumetric systems are sensitive to dead volume corrections and gas compressibility factors, whereas gravimetric systems require precise optimism, buoyancy, and balance calibrations. Differences in these operational principles can lead to systematic discrepancies when comparing data across laboratories, emphasizing the need for standardized testing methodologies and proper calibration of each measurement setup[206–208].

Instrument calibration

Accurate and reproducible adsorption measurements rely heavily on the precise calibration of sensors, valves, and measuring devices within the experimental system[208,209]. Over time, pressure transducers, temperature sensors, and microbalances can drift from their calibrated states, introducing systematic errors in data acquisition. Moreover, mechanical instabilities, such as small leaks, vibrations, or micro-shifts in fittings, can cause measurement fluctuations, especially during long-term isotherm recording. Regular instrument maintenance, leak testing, and periodic calibration using certified standards are essential practices to ensure consistency and reproducibility in adsorption data[210–212].

(*Pressure/Temperature control accuracy*) Maintaining stable and precise pressure and temperature conditions is crucial for reliable adsorption measurements, particularly within the practical hydrogen storage range of 0–50°C. Even small deviations in temperature can significantly alter gas density and adsorption equilibria at high pressure, leading to noticeable discrepancies in reported capacities. Similarly, inaccurate or unstable pressure regulation can distort adsorption and desorption isotherms, especially at high pressures near 200 bar. To minimize these effects, advanced temperature control systems (e.g., thermostated baths or jacketed reactors) and high-precision pressure transducers should be used, along with continuous monitoring and correction of environmental fluctuations[210,211].

Sample mass measurement

View Article Online
DOI: 10.1039/D5SE01539A

The accuracy of the sample mass measurement is another critical factor influencing reproducibility, as even minor weighing errors can lead to substantial deviations in the calculated hydrogen uptake per gram of adsorbent. Issues such as moisture absorption, electrostatic charge, or balance drift can introduce inconsistencies, particularly when dealing with small sample masses typical of MOFs and other porous materials. To reduce uncertainty, samples should be weighed immediately after activation under controlled, inert conditions using high-precision analytical balances. Implementing standardized weighing protocols and repeating mass measurements before and after adsorption tests can further enhance data reliability and comparability across experiments [213,214].

Proposed best-practice workflow:

(1) Pre-check: verify sample activation (residual solvent/moisture) and document batch history; (2) Instrument validation: leak test, dead-volume/buoyancy calibration, and EOS/fugacity settings for high-pressure H_2; (3) Measurement: define uptake basis (excess vs total), enforce equilibrium criteria, and perform replicate runs; (4) Validation: cross-check with a reference material and/or an orthogonal method; (5) Reporting: provide full conditions, uncertainty estimates, and raw isotherm data to enable independent verification.

5. Standardization Strategies and Best Practices for Improved Reproducibility

Ensuring reproducible adsorption measurements and reliable characterization of porous materials requires a combination of standardized sample preparation, instrument calibration, and harmonized measurement protocols. Uniform pretreatment procedures, including controlled thermal activation, vacuum drying, and solvent exchange, are essential to achieve a consistent surface state, while handling samples in inert atmospheres prevents moisture uptake and contamination. Instrumental stability is maintained through regular calibration of pressure transducers, temperature sensors, and balances, alongside leak testing and vibration control,

View Article Online
DOI: 10.1039/D5SE01539A

ensuring accurate measurement of hydrogen uptake under precise pressure and temperature conditions. Standardized measurement protocols, such as specifying adsorbate type, temperature, equilibration time, and data reduction methods for BET and pore size analysis, further enhance comparability across studies. Finally, rigorous quality control and transparent reporting covering sample mass, activation parameters, instrument settings, and analytical models allow researchers to benchmark results against reference materials and adhere to community best practices, thereby improving reproducibility and reliability in hydrogen storage research.

5.1. Proposed Standard Operating Procedures (SOP)

A standardized protocol for hydrogen adsorption measurements should specify sample pretreatment and calibration steps tailored to each material type, including precise vacuum and thermal activation conditions such as evacuation pressure, ramp rate, activation temperature, and duration. Proper post-activation handling, such as using inert atmosphere, desiccators, or sealed vials, is essential to prevent moisture uptake and contamination. Standardizing these procedures reduces variability and ensures adsorption measurements reflect intrinsic material properties. Furthermore, accurate temperature control during pretreatment and measurement is also crucial for reproducibility; the acceptable operating range and calibration intervals for temperature sensors should be clearly defined. Uniform calibration of instruments—including pressure transducers, thermocouples, balances, and vacuum gauges—should follow standard procedures with specified frequency and reference standards. Hence, implementing certification programs for laboratories that require adherence to these standardized operating protocols, regular calibration, proficiency testing, and inter-laboratory comparisons further improves reproducibility and data reliability across facilities, enabling credible benchmarking of hydrogen storage materials.

View Article Online
DOI: 10.1039/D5SE01539A

5.2. Need for Open Data Repositories and Shared Platforms

The adoption of standardized data formats is essential to facilitate reproducibility and cross-comparison in hydrogen storage research. Platforms such as the H_2 Storage Data Repository and AiF(Adsorption Information Format) provide structured frameworks for recording experimental results, ensuring that critical information, including adsorption isotherms, activation conditions, and instrument parameters, is reported consistently. Standardized formats reduce ambiguity, simplify data integration, and enable automated analysis across multiple studies, making it easier for researchers to evaluate material performance and identify trends in a reproducible manner.

5.3. Proposal for Reproducibility Evaluation Metrics

Assessing reproducibility in hydrogen adsorption measurements requires quantifying both intra-laboratory and inter-laboratory variability. Intra-laboratory standard deviation measures the consistency of repeated measurements within the same facility and reflects the precision of sample preparation, instrument operation, and measurement protocols. Inter-laboratory standard deviation, on the other hand, compares results obtained by different laboratories under similar experimental conditions, highlighting systematic differences arising from instrument types, calibration practices, or procedural variations. Together, these metrics provide a clear picture of how reliably adsorption data can be reproduced within and across research groups.

The coefficient of variation (CV), calculated as the ratio of the standard deviation to the mean, offers a normalized measure of reproducibility that allows comparison across different materials and experimental conditions. A low CV indicates high measurement precision and strong reproducibility, while a high CV signals potential issues in sample handling, instrument performance, or measurement methodology. Using CV as a standard metric enables researchers

View Article Online
DOI: 10.1039/D5SE01539A

to evaluate improvements in experimental protocols quantitatively, benchmark performance across laboratories, and establish acceptable tolerance limits for hydrogen adsorption studies. Reproducibility evaluation also requires systematic analysis of repeated measurements on the same sample to detect trends, anomalies, or drift in adsorption behavior. This involves performing multiple adsorption–desorption cycles under identical conditions and comparing the resulting isotherms for deviations in uptake, hysteresis, or equilibrium pressure. Consistent results across repeated measurements indicate reliable sample preparation, stable instrument performance, and minimal environmental interference. Incorporating such analyses into standard reporting ensures that the reported hydrogen capacities are robust, representative, and comparable across studies.

6. Current Challenges and Future Outlook

One of the foremost challenges in hydrogen storage research is achieving a balance between high adsorption performance and reproducibility. Materials that exhibit exceptional hydrogen uptake under ideal laboratory conditions may display variability when measured across different laboratories or under slightly altered conditions. Ensuring that high-capacity adsorbents maintain consistent performance across practical environments, including varying temperatures, pressures, and humidity, is essential for their real-world deployment. Standardized measurement protocols and robust sample handling procedures are therefore critical to bridging the gap between laboratory performance and practical applicability[197].

Hydrogen storage materials must demonstrate long-term stability under repeated adsorption–desorption cycles to be viable for commercial use. Factors such as framework degradation, pore collapse, or adsorption site poisoning can reduce uptake over time. Predicting material lifetime and quantifying cycle stability require systematic testing under realistic operating conditions and the development of accelerated aging protocols. Reliable lifetime data not only

View Article Online
DOI: 10.1039/D5SE01539A

informs material selection but also enables engineers to design storage systems with predictable performance and minimal maintenance requirements.

Artificial intelligence (AI) and machine learning techniques, such as Bayesian optimization, are increasingly being used to accelerate the discovery of high-performance hydrogen storage materials. However, the predictive power of AI models depends heavily on the quality and reproducibility of the underlying experimental data. Integrating AI-driven design with standardized and reproducible experimentation ensures that model predictions are reliable and actionable. This synergy can guide both material synthesis and measurement protocols, enabling more efficient identification of promising candidates while minimizing experimental trial-and-error[215].

7. Conclusion

Research on physisorption-based hydrogen storage materials such as metal-organic frameworks (MOFs), covalent organic frameworks (COFs), and porous carbons has been extensive, and these materials continue to attract significant interest due to their high surface areas, tunable pore structures, and light weight. Although cryogenic temperatures enable high hydrogen uptake, practical hydrogen storage at ambient temperatures (0–50 °C) remains a critical challenge, as storage capacities drop markedly compared to those at low temperatures. To address this limitation, various strategies have been pursued to enhance hydrogen binding energy on these adsorbents, thereby retaining hydrogen molecules at or near room temperature. These include metal doping, functionalization, pore-size and shape optimization, and combination with catalytic processes. Such efforts have yielded promising improvements in adsorption capacity under moderate temperature and pressure conditions. However, among the existing literature, some reported ambient-temperature hydrogen storage capacities appear to approach or even exceed values typically observed only at cryogenic temperatures (around 77

View Article Online
DOI: 10.1039/D5SE01539A

K). These unusually high adsorption results are often unreproducible and may be attributed to measurement artifacts, experimental errors, or non-equilibrium effects rather than genuine physisorption phenomena. Recognizing these challenges, this review emphasizes the critical importance of rigorous experimental protocols to minimize potential sources of error. Key factors include standardized sample preparation, precise control of activation and measurement conditions, consistent instrument calibration, and transparent reporting of procedural details. By adopting such systematic approaches, the hydrogen storage community can improve data reliability, enable meaningful comparisons across studies, and accelerate the development of truly viable ambient-temperature storage materials. Ultimately, advancing practical hydrogen storage solutions depends not only on innovative materials design but also equally on establishing reproducible methodologies and collaborative data sharing. These combined efforts will help bridge the gap between promising laboratory discoveries and scalable energy technologies essential for a sustainable hydrogen economy.

Table 5. Summarization of room-temperature hydrogen storage capacity and reproducibility challenges in MOFs, COFs, and Carbon Materials.

Material class	**Porous carbons** (AC, CNTs, graphene)	**MOFs**	**COFs**
Realistic capacity at ambient T (reproducible/ typical experimental)	Typically near the **lower end** of the reported spread; broadly reproducible outcomes are dominated by weak physisorption and pore-size distribution (often **sub-wt%** under common conditions; see spread in Table 5).	Typical experimental RT capacities cluster near the **lower–mid** part of the reported span; conventional MOFs often remain limited at RT without strong binding sites (see Table 5).	**Experimental** RT capacity is currently limited (Table 5: **~0.1–0.5 wt%**).
High-claim outliers (controversial / needs verification)	Reports approaching the **upper end**of the spread (Table 5 shows up to ~7 wt%) should be treated as **outliers** unless independently replicated with clear uptake definitions and rigorous high-pressure corrections.	Values near the **upper end** of the spread (Table 5 up to ~4 wt%) are often associated with **OMS** or **spillover-labelled** strategies and should be explicitly flagged for verification because spillover behavior is frequently inconsistent.	Any experimental-looking high capacities must be flagged if they are based on limited datasets or unclear definitions; many high numbers in the COF section are in fact theoretical predictions.
Computational-only " upper bound" (not experimental)	Many "enhanced CNT" claims are theoretical and assume ideal packing/defect-free tubes and perfectly dispersed dopants; these should be flagged as computational-only when applicable.	DFT/GCMC often predicts higher RT uptake than experiments; such predictions must be labelled computational-only and not mixed with experimental "realistic" ranges.	**Up to ~8.5 wt% (theoretical)**is reported in Table 5; several COF systems are predicted to reach ~5–7 wt% at 298 K and 100 bar under idealized conditions.

View Article Online
DOI: 10.1039/D5SE01539A

Typical/target Qst (kJ/mol) in this review	**~4–7**(typical)	**~5–8 (without OMS)**; **~10–15 (with OMS)**	**~6–10**(typical theoretical); in some designs **very high Qst (~50, theoretical extreme)** is mentioned in Table 5
What raises Qst / capacity	Heteroatom/metal doping, pore-size tuning (ultramicropores), defect engineering (but may introduce irreversible components)	**Open metal sites (OMS)**, metal decoration, (reported) spillover; pore-size/surface area optimization	Pore confinement+functionalization; metal incorporation may strongly increase Qst (e.g., Pd–H_2 interactions were predicted to raise Qst from ~6 to ~23 kJ/mol in one COF case, but experimental realization remained challenging).
Main reproducibility challenges (dominant causes)	**Surface heterogeneity**, **batch-to-batch variation**, **impurities**, **pore-size dispersion**(broad PSD makes outcomes lab-dependent)	**Activation sensitivity**, **framework defects**, **metal-site availability variability**, **spillover inconsistency**	**Mostly simulation-based literature**, **crystallinity control**, **stacking disorder**, **pore collapse**, **residual solvents**

To provide an across-class benchmark, Table 5 summarizes ambient-temperature H_2 storage performance in porous carbons, MOFs, and COFs by separating realistic (reproducible) experimental ranges from controversial high-claim outliers and computational-only upper bounds. Across all three classes, improving room-temperature uptake generally requires increasing adsorption enthalpy (Qst); however, the dominant reproducibility bottlenecks differ: porous carbons are limited by surface heterogeneity and batch variability, MOFs by activation sensitivity/defects/variable accessible metal sites and inconsistent spillover-labelled behavior, and COFs by crystallinity/stacking disorder/pore collapse and the fact that many high capacities remain simulation-based.

Acknowledgments

This work was supported by the National Research Foundation of Korea (NRF) grant program funded by the Korean Government (MSI) (Nos. 2021M3I3A1084909, RS-2025-02982993). S.K. acknowledges the Brain Pool Program funded by the Ministry of Science and ICT through the National Research Foundation of Korea (no. RS-2024-00399272). M.M. acknowledges the Brain Pool Program funded by the Ministry of Science and ICT through the National Research Foundation of Korea (no. RS-2023-00282300).

View Article Online
DOI: 10.1039/D5SE01539A

References

[1] S. Ahamed, G. L. Galford, B. Panikkar, D. Rizzo, J. C. Stephens, *Energy Policy* **2024**, *190*, 114103.

[2] O. Ellabban, H. Abu-Rub, F. Blaabjerg, *Renew. Sustain. Energy Rev.* **2014**, *39*, 748.

[3] Q. Hassan, S. Algburi, A. Z. Sameen, M. Jaszczur, H. M. Salman, *Environ. Syst. Decis.* **2024**, *44*, 327.

[4] S. Ahmad, A. Ullah, A. Samreen, M. Qasim, K. Nawaz, W. Ahmad, A. Alnaser, A. M. Kannan, M. Egilmez, *J. Energy Storage* **2024**, *101*, 113733.

[5] A. Alamiery, *ChemPhysMater* **2023**.

[6] M. Hirscher, L. Zhang, H. Oh, *Appl. Phys. A* **2023**, *129*, 112.

[7] M. Alsunousi, E. Kayabasi, *Int. J. Hydrogen Energy* **2024**, *54*, 1169.

[8] T. T. Le, P. Sharma, B. J. Bora, V. D. Tran, T. H. Truong, H. C. Le, P. Q. P. Nguyen, *Int. J. Hydrogen Energy* **2024**, *54*, 791.

[9] L. Ge, B. Zhang, W. Huang, Y. Li, L. Hou, J. Xiao, Z. Mao, X. Li, *J. Energy Storage* **2024**, *75*, 109307.

[10] V. Sridevi, D. V. Surya, B. R. Reddy, M. Shah, R. Gautam, T. H. Kumar, H. Puppala, K. S. Pritam, T. Basak, *Int. J. Hydrogen Energy* **2024**, *52*, 507.

[11] M. A. Green, In *AIP Conference Proceedings*, AIP, **2006**, pp. 319–326.

[12] E. Ohaeri, U. Eduok, J. Szpunar, *Int. J. Hydrogen Energy* **2018**, *43*, 14584.

[13] H. Sun, Z. Wang, Q. Meng, S. White, *Int. J. Hydrogen Energy* **2025**, *105*, 10.

[14] H. Li, X. Cao, Y. Liu, Y. Shao, Z. Nan, L. Teng, W. Peng, J. Bian, *Energy Reports* **2022**, *8*, 6258.

[15] A. Z$\hat{\text{a}}$ttel, *Naturwissenschaften* **2004**, *91*, 157.

[16] M. R. Usman, *Renew. Sustain. Energy Rev.* **2022**, *167*, 112743.

[17] D. J. Durbin, C. Malardier-Jugroot, *Int. J. Hydrogen Energy* **2013**, *38*, 14595.

[18] E. Rivard, M. Trudeau, K. Zaghib, *Materials (Basel).* **2019**, *12*, 1973.

[19] S. Niaz, T. Manzoor, A. H. Pandith, *Renew. Sustain. Energy Rev.* **2015**, *50*, 457.

[20] R. K. Ahluwalia, T. Q. Hua, J.-K. Peng, S. Lasher, K. McKenney, J. Sinha, M. Gardiner, *Int. J. Hydrogen Energy* **2010**, *35*, 4171.

[21] L. G. Scanlon, W. A. Feld, P. B. Balbuena, G. Sandi, X. Duan, K. A. Underwood, N. Hunter, J. Mack, M. A. Rottmayer, M. Tsao, *J. Phys. Chem. B* **2009**, *113*, 4708.

View Article Online
DOI: 10.1039/D5SE01539A

[22] S. Park, R. Muhammad, H. Oh, *Chem. Eng. J.* **2025**, *516*, 164060.

[23] S. Pinjari, T. Bera, E. Kjeang, *Nanoenergy Adv.* **2025**, *5*, 5.

[24] A. Jamil, M. Shahbaz, *Curr. Opin. Green Sustain. Chem.* **2025**, *54*, 101040.

[25] R. Murugavel, A. A. Rownaghi, P. A. Webley, F. Rezaei, *Energy & Fuels* **2025**, *39*, 18251.

[26] J. Zheng, C.-G. Wang, H. Zhou, E. Ye, J. Xu, Z. Li, X. J. Loh, *Research* **2021**, *2021*.

[27] G. J. Kubas, *J. Organomet. Chem.* **2001**, *635*, 37.

[28] F. Costanzo, P. L. Silvestrelli, F. Ancilotto, *J. Chem. Theory Comput.* **2012**, *8*, 1288.

[29] Q. Lai, M. Paskevicius, D. A. Sheppard, C. E. Buckley, A. W. Thornton, M. R. Hill, Q. Gu, J. Mao, Z. Huang, H. K. Liu, Z. Guo, A. Banerjee, S. Chakraborty, R. Ahuja, K. Aguey-Zinsou, *ChemSusChem* **2015**, *8*, 2789.

[30] Fundamentals of adsorption technology, **2021**, pp. 1–70.

[31] M. Ahmed Alsharif, In *Adsorption - Fundamental Mechanisms and Applications*, IntechOpen, **2025**.

[32] L. ZHOU, Y. ZHOU, Y. SUN, *Int. J. Hydrogen Energy* **2006**, *31*, 259.

[33] Z. Yang, Y. Xia, R. Mokaya, *J. Am. Chem. Soc.* **2007**, *129*, 1673.

[34] A. G. Wong-Foy, A. J. Matzger, O. M. Yaghi, *J. Am. Chem. Soc.* **2006**, *128*, 3494.

[35] A. Song, J. Wu, J. Sun, W. Liang, Y. Li, Z. Ling, G. Zhang, X. Zhao, *Energy & Fuels* **2024**, *38*, 17146.

[36] W. Shi, X. Jin, C. Zhang, X. Zhang, X. Liu, Y. Gao, W. Ding, H. Gao, A. Li, *Int. J. Hydrogen Energy* **2024**, *83*, 432.

[37] B. Abebe, H. C. A. Murthy, E. Amare, *J. Encapsulation Adsorpt. Sci.* **2018**, *8*, 225.

[38] T. Yildirim, M. Hartman, *Phys. Rev. Lett.* **2005**, *95*, 215504.

[39] T. Mueller, G. Ceder, *J. Phys. Chem. B* **2005**, *109*, 17974.

[40] Z. Chen, K. O. Kirlikovali, K. B. Idrees, M. C. Wasson, O. K. Farha, *Chem* **2022**, *8*, 693.

[41] A. W. Thornton, K. M. Nairn, J. M. Hill, A. J. Hill, M. R. Hill, *J. Am. Chem. Soc.* **2009**, *131*, 10662.

[42] S. Bosu, N. Rajamohan, *Int. J. Hydrogen Energy* **2024**, *52*, 352.

[43] M. Rzepka, P. Lamp, M. A. de la Casa-Lillo, *J. Phys. Chem. B* **1998**, *102*, 10894.

[44] L. S. Blankenship, N. Balahmar, R. Mokaya, *Nat. Commun.* **2017**, *8*, 1545.

[45] L. J. Murray, M. Dincă, J. R. Long, *Chem. Soc. Rev.* **2009**, *38*, 1294.

View Article Online
DOI: 10.1039/D5SE01539A

[46] H. Kim, M. Jung, J. Park, T. Park, J. Park, H. Lee, B. G. Ghule, J.-H. Jang, R. Muhammad, S. Kumar, H. Oh, *Carbon N. Y.* **2024**, *230*, 119674.

[47] H. Frost, T. Düren, R. Q. Snurr, *J. Phys. Chem. B* **2006**, *110*, 9565.

[48] A. W. Thornton, S. A. Furman, K. M. Nairn, A. J. Hill, J. M. Hill, M. R. Hill, *Microporous Mesoporous Mater.* **2013**, *167*, 188.

[49] P. K. Panigrahi, B. Chandu, M. R. Motapothula, N. Puvvada, *Energy & Fuels* **2024**, *38*, 2630.

[50] E. Boateng, A. Chen, *Mater. Today Adv.* **2020**, *6*, 100022.

[51] C. Li, Z. Yang, H. Luo, T. Yang, L. Tong, Y. Yuan, C. Yuan, R. Chahine, J. Xiao, *Fuel* **2025**, *381*, 133398.

[52] P. García-Holley, B. Schweitzer, T. Islamoglu, Y. Liu, L. Lin, S. Rodriguez, M. H. Weston, J. T. Hupp, D. A. Gómez-Gualdrón, T. Yildirim, O. K. Farha, *ACS Energy Lett.* **2018**, *3*, 748.

[53] S. E. Bambalaza, H. W. Langmi, R. Mokaya, N. M. Musyoka, L. E. Khotseng, *ACS Appl. Mater. Interfaces* **2020**, *12*, 24883.

[54] L. Schlapbach, A. Züttel, *Nature* **2001**, *414*, 353.

[55] S. Kumar, B. Mohan, B. Musikavanhu, X. Wang, R. Muhammad, X. Yang, P. Ren, *Coord. Chem. Rev.* **2025**, *524*, 216286.

[56] S. Kumar, R. Muhammad, A. Amhamed, H. Oh, *Coord. Chem. Rev.* **2025**, *522*, 216230.

[57] H. Kim, S. H. So, R. Muhammad, H. Oh, *Int. J. Hydrogen Energy* **2024**, *50*, 1616.

[58] J. A. Villajos, R. Balderas-Xicohténcatl, A. N. Al Shakhs, Á. Berenguer-Murcia, C. E. Buckley, D. Cazorla-Amorós, G. Charalambopoulou, F. Couturas, F. Cuevas, D. Fairen-Jimenez, K. N. Heinselman, T. D. Humphries, S. Kaskel, H. Kim, J. P. Marco-Lozar, H. Oh, P. A. Parilla, M. Paskevicius, I. Senkovska, S. Shulda, J. Silvestre-Albero, T. Steriotis, C. Tampaxis, M. Hirscher, M. Maiwald, *ChemPhysChem* **2024**, *25*.

[59] L. A. M. Mahmoud, J. L. Rowlandson, D. J. Fermin, V. P. Ting, S. Nayak, *RSC Appl. Interfaces* **2025**.

[60] Y. Chen, G. Zhao, S. Yoon, P. Habibi, C. S. Hong, S. Li, O. A. Moultos, P. Dey, T. J. H. Vlugt, Y. G. Chung, *ACS Appl. Mater. Interfaces* **2024**, *16*, 61995.

[61] F. Qureshi, M. Yusuf, S. Ahmed, M. Haq, A. M. Alraih, T. Hidouri, H. Kamyab, D.-V.

View Article Online
DOI: 10.1039/D5SE01539A

N. Vo, H. Ibrahim, *Energy* **2024**, *309*, 132855.

[62] H. Vo Thanh, Z. Dai, Z. Du, H. Yin, B. Yan, M. R. Soltanian, T. Xiao, B. McPherson, L. Abualigah, *Int. J. Hydrogen Energy* **2024**, *57*, 1000.

[63] H. Wang, H. J. Lin, W. T. Cai, L. Z. Ouyang, M. Zhu, *J. Alloys Compd.* **2016**, *658*, 280.

[64] S. Lee, K. H. Oh, S. Ravi, Y. Bae, *J. Ind. Eng. Chem.* **2024**.

[65] T. H. Kim, J. Bae, T. H. Lee, J. Hwang, J. H. Jung, D. K. Kim, J. S. Lee, D. O. Kim, Y. H. Lee, J. Ihm, *Nano Energy* **2016**, *27*, 402.

[66] R. S. Rajaura, S. Srivastava, V. Sharma, P. K. Sharma, C. Lal, M. Singh, H. S. Palsania, Y. K. Vijay, *Int. J. Hydrogen Energy* **2016**, *41*, 9454.

[67] N. Thaweelap, P. Plerdsranoy, Y. Poo-arporn, P. Khajondetchairit, S. Suthirakun, I. Fongkaew, P. Hirunsit, N. Chanlek, O. Utke, A. Pangon, R. Utke, *Fuel* **2021**, *288*, 119608.

[68] S.-Y. Lee, S.-J. Park, *Int. J. Hydrogen Energy* **2011**, *36*, 8381.

[69] S. H. Aboutalebi, S. Aminorroaya-Yamini, I. Nevirkovets, K. Konstantinov, H. K. Liu, *Adv. Energy Mater.* **2012**, *2*, 1439.

[70] B. Adeniran, R. Mokaya, *J. Mater. Chem. A* **2015**, *3*, 5148.

[71] G. Chen, Y. Zhang, J. Chen, X. Guo, Y. Zhu, L. Li, *Nanotechnology* **2018**, *29*, 265705.

[72] A. A. S. Nair, R. Sundara, N. Anitha, *Int. J. Hydrogen Energy* **2015**, *40*, 3259.

[73] A. A. S. Nair, R. Sundara, *J. Phys. Chem. C* **2016**, *120*, 9612.

[74] R. Ströbel, J. Garche, P. T. Moseley, L. Jörissen, G. Wolf, *J. Power Sources* **2006**, *159*, 781.

[75] M. Mohan, V. K. Sharma, E. A. Kumar, V. Gayathri, *Energy Storage* **2019**, *1*.

[76] T. Ramesh, N. Rajalakshmi, K. S. Dhathathreyan, *J. Energy Storage* **2015**, *4*, 89.

[77] M. K. Yadav, N. Panwar, S. Singh, P. Kumar, *Int. J. Hydrogen Energy* **2020**, *45*, 19561.

[78] S. Rezaie, D. M. J. Smeulders, A. Luna-Triguero, *Chem. Eng. J.* **2023**, *476*, 146525.

[79] H. Jung, K. T. Park, M. N. Gueye, S. H. So, C. R. Park, *Int. J. Hydrogen Energy* **2016**, *41*, 5019.

[80] S. Nachimuthu, P.-J. Lai, E. G. Leggesse, J.-C. Jiang, *Sci. Rep.* **2015**, *5*, 16797.

[81] B. P. Vinayan, R. Nagar, S. Ramaprabhu, *J. Mater. Chem. A* **2013**, *1*, 11192.

[82] C. Zhou, J. A. Szpunar, *ACS Appl. Mater. Interfaces* **2016**, *8*, 25933.

View Article Online
DOI: 10.1039/D5SE01539A

[83] S. S. Samantaray, V. Sangeetha, S. Abinaya, S. Ramaprabhu, *Int. J. Hydrogen Energy* **2018**, *43*, 8018.

[84] Y. Wang, C. X. Guo, X. Wang, C. Guan, H. Yang, K. Wang, C. M. Li, *Energy Environ. Sci.* **2011**, *4*, 195.

[85] X. Li, S. Sun, J. Zhang, K. Luo, P. Gao, T. Wu, S. Du, Y. Wang, X. Zhou, L. Sha, Y. Yang, P. Yang, Y. Wang, Y. Chen, *RSC Adv.* **2016**, *6*, 93238.

[86] C. I. Contescu, C. M. Brown, Y. Liu, V. V. Bhat, N. C. Gallego, *J. Phys. Chem. C* **2009**, *113*, 5886.

[87] A. Ansón, E. Lafuente, E. Urriolabeitia, R. Navarro, A. M. Benito, W. K. Maser, M. T. Martínez, *J. Phys. Chem. B* **2006**, *110*, 6643.

[88] C. M. Ghimbeu, C. Zlotea, R. Gadiou, F. Cuevas, E. Leroy, M. Latroche, C. Vix-Guterl, *J. Mater. Chem.* **2011**, *21*, 17765.

[89] M. Hirscher, M. Becher, M. Haluska, F. von Zeppelin, X. Chen, U. Dettlaff-Weglikowska, S. Roth, *J. Alloys Compd.* **2003**, *356–357*, 433.

[90] N. P. Stadie, J. J. Purewal, C. C. Ahn, B. Fultz, *Langmuir* **2010**, *26*, 15481.

[91] H. Oh, T. Gennett, P. Atanassov, M. Kurttepeli, S. Bals, K. E. Hurst, M. Hirscher, *Microporous Mesoporous Mater.* **2013**, *177*, 66.

[92] R. Campesi, F. Cuevas, R. Gadiou, E. Leroy, M. Hirscher, C. Vix-Guterl, M. Latroche, *Carbon N. Y.* **2008**, *46*, 206.

[93] J. Lyu, V. Kudiiarov, A. Lider, *Nanomaterials* **2020**, *10*, 255.

[94] S. ullah Rather, *Int. J. Hydrogen Energy* **2020**, *45*, 4653.

[95] K. Jastrzębski, P. Kula, *Materials (Basel).* **2021**, *14*, 2499.

[96] T. Das, S. Banerjee, K. Dasgupta, J. B. Joshi, V. Sudarsan, *RSC Adv.* **2015**, *5*, 41468.

[97] M. Aghababaei, A. A. Ghoreyshi, K. Esfandiari, *Int. J. Hydrogen Energy* **2020**, *45*, 23112.

[98] E. Mosquera-Vargas, R. Tamayo, M. Morel, M. Roble, D. E. Díaz-Droguett, *Heliyon* **2021**, *7*, e08494.

[99] A. Reyhani, S. Z. Mortazavi, S. Mirershadi, A. Z. Moshfegh, P. Parvin, A. N. Golikand, *J. Phys. Chem. C* **2011**, *115*, 6994.

[100] M. Mananghaya, D. Yu, G. N. Santos, E. Rodulfo, *Sci. Rep.* **2016**, *6*, 27370.

[101] M. Sevilla, R. Mokaya, *Energy Environ. Sci.* **2014**, *7*, 1250.

[102] S. Kaskun, Y. Akinay, M. Kayfeci, *Int. J. Hydrogen Energy* **2020**, *45*, 34949.

View Article Online
DOI: 10.1039/D5SE01539A

[103] R. Naresh Muthu, S. Rajashabala, R. Kannan, *Renew. Energy* **2016**, *85*, 387.

[104] A. Ariharan, B. Viswanathan, V. Nandhakumar, *Int. J. Hydrogen Energy* **2018**, *43*, 5077.

[105] S. V. Sawant, M. D. Yadav, S. Banerjee, A. W. Patwardhan, J. B. Joshi, K. Dasgupta, *Int. J. Hydrogen Energy* **2021**, *46*, 39297.

[106] S. V. Sawant, S. Banerjee, A. W. Patwardhan, J. B. Joshi, K. Dasgupta, *Int. J. Hydrogen Energy* **2020**, *45*, 13406.

[107] M. Sankaran, B. Viswanathan, *Carbon N. Y.* **2007**, *45*, 1628.

[108] N. F. Tajul Arifin, N. Yusof, N. A. H. Md Nordin, J. Jaafar, A. F. Ismail, F. Aziz, W. N. Wan Salleh, *Int. J. Hydrogen Energy* **2021**, *46*, 31084.

[109] P. Pei, M. B. Whitwick, W. L. Sun, G. Quan, M. Cannon, E. Kjeang, *Nanoscale* **2017**, *9*, 4143.

[110] H. Lee, J. Ihm, M. L. Cohen, S. G. Louie, *Nano Lett.* **2010**, *10*, 793.

[111] B.-J. Kim, S.-J. Park, *Int. J. Hydrogen Energy* **2011**, *36*, 648.

[112] Y. Liu, Z. Zhang, T. Wang, *Int. J. Hydrogen Energy* **2018**, *43*, 11120.

[113] S. S. Samantaray, P. Anees, V. Bhaghavathi Parambath, R. S, *Acta Mater.* **2021**, *215*, 117040.

[114] S. Rather, *Int. J. Hydrogen Energy* **2021**, *46*, 17793.

[115] U. Khalilov, U. Uljayev, K. Mehmonov, P. Nematollahi, M. Yusupov, E. Neyts, *Int. J. Hydrogen Energy* **2024**, *55*, 604.

[116] S. Mishra, N. Luhadiya, S. I. Kundalwal, *Carbon N. Y.* **2023**, *207*, 23.

[117] M. Shi, L. Bi, X. Huang, Z. Meng, Y. Wang, Z. Yang, *Appl. Surf. Sci.* **2020**, *534*, 147606.

[118] B. Assfour, S. Leoni, G. Seifert, I. A. Baburin, *Adv. Mater.* **2011**, *23*, 1237.

[119] A. Ariharan, B. Viswanathan, V. Nandhakumar, *Int. J. Hydrogen Energy* **2016**, *41*, 3527.

[120] P. Plerdsranoy, N. Thaweelap, Y. Poo-arporn, P. Khajondetchairit, S. Suthirakun, I. Fongkaew, N. Chanlek, O. Utke, A. Pangon, R. Utke, *Int. J. Hydrogen Energy* **2021**, *46*, 5427.

[121] Y. Li, R. T. Yang, *J. Phys. Chem. C* **2007**, *111*, 11086.

[122] L. Wang, R. T. Yang, *J. Phys. Chem. C* **2008**, *112*, 12486.

[123] H. Lee, D. G. Park, J. Park, Y. Kim, J. K. Kang, *Adv. Energy Mater.* **2023**, *13*.

View Article Online
DOI: 10.1039/D5SE01539A

[124] W. Zhao, V. Fierro, C. Zlotea, M. T. Izquierdo, C. Chevalier-César, M. Latroche, A. Celzard, *Int. J. Hydrogen Energy* **2012**, *37*, 5072.

[125] N. Erruboyana, G. Zollo, *Carbon N. Y.* **2023**, *215*, 118388.

[126] D. Minami, T. Ohkubo, Y. Kuroda, K. Sakai, H. Sakai, M. Abe, *Int. J. Hydrogen Energy* **2010**, *35*, 12398.

[127] R. Murugavel, A. A. Rownaghi, F. Rezaei, *ACS Appl. Nano Mater.* **2024**, *7*, 23733.

[128] Y. H. Hu, L. Zhang, *Adv. Mater.* **2010**, *22*.

[129] H. Montes-Andrés, G. Orcajo, C. Martos, J. A. Botas, G. Calleja, *Int. J. Hydrogen Energy* **2019**, *44*, 18205.

[130] J. L. C. Rowsell, O. M. Yaghi, *Angew. Chemie Int. Ed.* **2005**, *44*, 4670.

[131] H. Li, M. Eddaoudi, M. O'Keeffe, O. M. Yaghi, *Nature* **1999**, *402*, 276.

[132] K. Sumida, M. R. Hill, S. Horike, A. Dailly, J. R. Long, *J. Am. Chem. Soc.* **2009**, *131*, 15120.

[133] H. Chun, H. Jung, G. Koo, H. Jeong, D.-K. Kim, *Inorg. Chem.* **2008**, *47*, 5355.

[134] L. Pan, M. B. Sander, X. Huang, J. Li, M. Smith, E. Bittner, B. Bockrath, J. K. Johnson, *J. Am. Chem. Soc.* **2004**, *126*, 1308.

[135] Q. Fang, G. Zhu, M. Xue, Q. Zhang, J. Sun, X. Guo, S. Qiu, S. Xu, P. Wang, D. Wang, Y. Wei, *Chem. – A Eur. J.* **2006**, *12*, 3754.

[136] J. Li, T. Furuta, H. Goto, T. Ohashi, Y. Fujiwara, S. Yip, *J. Chem. Phys.* **2003**, *119*, 2376.

[137] B. Kesanli, Y. Cui, M. R. Smith, E. W. Bittner, B. C. Bockrath, W. Lin, *Angew. Chemie Int. Ed.* **2005**, *44*, 72.

[138] Q. Fang, G. Zhu, Z. Jin, Y. Ji, J. Ye, M. Xue, H. Yang, Y. Wang, S. Qiu, *Angew. Chemie Int. Ed.* **2007**, *46*, 6638.

[139] D. Yuan, D. Zhao, D. Sun, H. Zhou, *Angew. Chemie Int. Ed.* **2010**, *49*, 5357.

[140] Z. Li, G. Zhu, G. Lu, S. Qiu, X. Yao, *J. Am. Chem. Soc.* **2010**, *132*, 1490.

[141] H. J. Park, M. P. Suh, *Chem. Commun.* **2012**, *48*, 3400.

[142] G. Orcajo, H. Montes-Andrés, J. A. Villajos, C. Martos, J. A. Botas, G. Calleja, *Int. J. Hydrogen Energy* **2019**, *44*, 19285.

[143] D. Dybtsev, C. Serre, B. Schmitz, B. Panella, M. Hirscher, M. Latroche, P. L. Llewellyn, S. Cordier, Y. Molard, M. Haouas, F. Taulelle, G. Férey, *Langmuir* **2010**, *26*, 11283.

View Article Online
DOI: 10.1039/D5SE01539A

[144] D. W. Kim, M. Jung, D. Y. Shin, N. Kim, J. Park, J.-H. Lee, H. Oh, C. S. Hong, *Chem. Eng. J.* **2024**, *489*, 151500.

[145] G. J. Kubas, *Proc. Natl. Acad. Sci.* **2007**, *104*, 6901.

[146] D. E. Jaramillo, H. Z. H. Jiang, H. A. Evans, R. Chakraborty, H. Furukawa, C. M. Brown, M. Head-Gordon, J. R. Long, *J. Am. Chem. Soc.* **2021**, *143*, 6248.

[147] M. T. Kapelewski, T. Runčevski, J. D. Tarver, H. Z. H. Jiang, K. E. Hurst, P. A. Parilla, A. Ayala, T. Gennett, S. A. FitzGerald, C. M. Brown, J. R. Long, *Chem. Mater.* **2018**, *30*, 8179.

[148] M. Dincă, A. Dailly, Y. Liu, C. M. Brown, D. A. Neumann, J. R. Long, *J. Am. Chem. Soc.* **2006**, *128*, 16876.

[149] Y. Yabuuchi, H. Furukawa, K. M. Carsch, R. A. Klein, N. V. Tkachenko, A. J. Huang, Y. Cheng, K. M. Taddei, E. Novak, C. M. Brown, M. Head-Gordon, J. R. Long, *J. Am. Chem. Soc.* **2024**, *146*, 22759.

[150] Y. Li, R. T. Yang, *J. Am. Chem. Soc.* **2006**, *128*, 726.

[151] Y. Li, F. H. Yang, R. T. Yang, *J. Phys. Chem. C* **2007**, *111*, 3405.

[152] Y. Li, R. T. Yang, *J. Am. Chem. Soc.* **2006**, *128*, 8136.

[153] A. K. Adhikari, K.-S. Lin, C.-S. Chang, *Res. Chem. Intermed.* **2015**, *41*, 7655.

[154] D. Rao, R. Lu, C. Xiao, E. Kan, K. Deng, *Chem. Commun.* **2011**, *47*, 7698.

[155] M. Hirscher, *Microporous Mesoporous Mater.* **2010**, *135*, 209.

[156] S. M. Luzan, A. V. Talyzin, *Microporous Mesoporous Mater.* **2011**, *139*, 216.

[157] R. Campesi, F. Cuevas, M. Latroche, M. Hirscher, *Phys. Chem. Chem. Phys.* **2010**, *12*, 10457.

[158] S. B. Kalidindi, H. Oh, M. Hirscher, D. Esken, C. Wiktor, S. Turner, G. Van Tendeloo, R. A. Fischer, *Chem. – A Eur. J.* **2012**, *18*, 10848.

[159] Y. Li, L. Xie, Y. Liu, R. Yang, X. Li, *Inorg. Chem.* **2008**, *47*, 10372.

[160] L. Xia, Q. Liu, *Comput. Mater. Sci.* **2017**, *126*, 176.

[161] P. Suksaengrat, V. Amornkitbamrung, P. Srepusharawoot, R. Ahuja, *ChemPhysChem* **2016**, *17*, 879.

[162] B. J. Bucior, N. S. Bobbitt, T. Islamoglu, S. Goswami, A. Gopalan, T. Yildirim, O. K. Farha, N. Bagheri, R. Q. Snurr, *Mol. Syst. Des. Eng.* **2019**, *4*, 162.

[163] J. Łuczak, M. Kroczewska, M. Baluk, J. Sowik, P. Mazierski, A. Zaleska-Medynska, *Adv. Colloid Interface Sci.* **2023**, *314*, 102864.

View Article Online
DOI: 10.1039/D5SE01539A

[164] M.-M. Xu, X.-J. Kong, T. He, X.-Q. Wu, L.-H. Xie, J.-R. Li, *Dalt. Trans.* **2019**, *48*, 9225.

[165] Y.-X. Sun, W.-Y. Sun, *Chinese Chem. Lett.* **2014**, *25*, 823.

[166] M. S. Salimi, H. Molavi, *Sci. Rep.* **2025**, *15*, 37255.

[167] C. McKinstry, E. J. Cussen, A. J. Fletcher, S. V. Patwardhan, J. Sefcik, *Cryst. Growth Des.* **2013**, *13*, 5481.

[168] J. Letwaba, U. O. Uyor, M. L. Mavhungu, N. O. Achuka, P. A. Popoola, *RSC Adv.* **2024**, *14*, 14233.

[169] V. Zeleňák, I. Saldan, *Nanomaterials* **2021**, *11*, 1638.

[170] R. Li, X. Han, Q. Liu, A. Qian, F. Zhu, J. Hu, J. Fan, H. Shen, J. Liu, X. Pu, H. Xu, B. Mu, *ACS Omega* **2022**, *7*, 20081.

[171] I. Cabria, M. J. López, J. A. Alonso, *Phys. Rev. B* **2008**, *78*, 205432.

[172] H. Zhao, Y. Guan, H. Guo, R. Du, C. Yan, *Mater. Res. Express* **2020**, *7*, 35506.

[173] S. Ghosh, J. K. Singh, *Int. J. Hydrogen Energy* **2019**, *44*, 1782.

[174] X.-D. Li, H.-P. Zang, J.-T. Wang, J.-F. Wang, H. Zhang, *J. Mater. Chem. A* **2014**, *2*, 18554.

[175] L. Zhao, B.-Z. Xu, J. Jia, H.-S. Wu, *Comput. Mater. Sci.* **2017**, *137*, 107.

[176] Z. Meng, H. Ma, Q. Wang, X. Yang, Y. Wang, X. Li, *Sci. China Technol. Sci.* **2024**, *67*, 3791.

[177] D. Cao, J. Lan, W. Wang, B. Smit, *Angew. Chemie Int. Ed.* **2009**, *48*, 4730.

[178] E. Klontzas, E. Tylianakis, G. E. Froudakis, *Nano Lett.* **2010**, *10*, 452.

[179] E. Klontzas, E. Tylianakis, G. E. Froudakis, *J. Phys. Chem. C* **2008**, *112*, 9095.

[180] J. L. Mendoza-Cortes, W. A. Goddard, H. Furukawa, O. M. Yaghi, *J. Phys. Chem. Lett.* **2012**, *3*, 2671.

[181] M. Djokic, J. L. Mendoza-Cortes, *Energy & Fuels* **2024**, *38*, 4711.

[182] X.-D. Li, J.-H. Guo, H. Zhang, X.-L. Cheng, X.-Y. Liu, *RSC Adv.* **2014**, *4*, 24526.

[183] Y. J. Choi, J. W. Lee, J. H. Choi, J. K. Kang, *Appl. Phys. Lett.* **2008**, *92*.

[184] S. B. Kalidindi, R. A. Fischer, *Phys. status solidi* **2013**, *250*, 1119.

[185] E. Klontzas, E. Tylianakis, G. E. Froudakis, *J. Phys. Chem. C* **2009**, *113*, 21253.

[186] B. W. J. Chen, M. Mavrikakis, *Nano Energy* **2019**, *63*, 103858.

[187] L. He, Y. B. Melnichenko, N. C. Gallego, C. I. Contescu, J. Guo, J. Bahadur, *Carbon N. Y.* **2014**, *80*, 82.

View Article Online
DOI: 10.1039/D5SE01539A

[188] A. Gatin, M. Grishin, N. Dokhlikova, S. Ozerin, S. Sarvadii, V. Kharitonov, B. Shub, *Nanomaterials* **2019**, *9*, 344.

[189] D. Van Lai, S. H. Nguyen, A. H. Nguyen, T. Van Nguyen, L. C. Dinh, P. D. Doan, T. T. Pham, V. H. T. Phung, M. Tonezzer, D. D. La, T. T. Nguyen, T. B. Tran, *RSC Adv.* **2025**, *15*, 31240.

[190] D. G. Madden, D. O'Nolan, N. Rampal, R. Babu, C. Çamur, A. N. Al Shakhs, S.-Y. Zhang, G. A. Rance, J. Perez, N. Pietro Maria Casati, C. Cuadrado-Collados, D. O'Sullivan, N. P. Rice, T. Gennett, P. Parilla, S. Shulda, K. E. Hurst, V. Stavila, M. D. Allendorf, J. Silvestre-Albero, A. C. Forse, N. R. Champness, K. W. Chapman, D. Fairen-Jimenez, *J. Am. Chem. Soc.* **2022**, *144*, 13729.

[191] A. S. Mekonnin, K. Wacławiak, M. Humayun, S. Zhang, H. Ullah, *Catalysts* **2025**, *15*, 260.

[192] W. Yuan, T. Wang, C. Wang, *Int. J. Hydrogen Energy* **2023**, *48*, 38389.

[193] H. Barthélémy, *Int. J. Hydrogen Energy* **2011**, *36*, 2750.

[194] M.-S. Lee, M. Park, H. Y. Kim, S.-J. Park, *Sci. Rep.* **2016**, *6*, 23224.

[195] C. Guerrero, J. C. Santamarina, *Int. J. Hydrogen Energy* **2024**, *95*, 417.

[196] A. Ansón, J. Jagiello, J. B. Parra, M. L. Sanjuán, A. M. Benito, W. K. Maser, M. T. Martínez, *J. Phys. Chem. B* **2004**, *108*, 15820.

[197] D. P. Broom, M. Hirscher, *ChemPhysChem* **2021**, *22*, 2141.

[198] V. Bhadariya, J. Kaur, P. Sapale, P. Rasane, J. Singh, *Int. J. Hydrogen Energy* **2024**, *67*, 681.

[199] W. A. van Rooijen, H. Hajibeygi, *Energy & Fuels* **2025**, *39*, 19600.

[200] Z. Qie, X. Zhang, Z. Wang, Z. Liu, H. Alhassawi, H. Li, G. Chen, G. Zhao, *J. Ind. Eng. Chem.* **2024**, *139*, 611.

[201] A. D. Lueking, R. T. Yang, N. M. Rodriguez, R. T. K. Baker, *Langmuir* **2004**, *20*, 714.

[202] N. Heinemann, J. Alcalde, J. M. Miocic, S. J. T. Hangx, J. Kallmeyer, C. Ostertag-Henning, A. Hassanpouryouzband, E. M. Thaysen, G. J. Strobel, C. Schmidt-Hattenberger, K. Edlmann, M. Wilkinson, M. Bentham, R. Stuart Haszeldine, R. Carbonell, A. Rudloff, *Energy Environ. Sci.* **2021**, *14*, 853.

[203] S. S. Kaye, A. Dailly, O. M. Yaghi, J. R. Long, *J. Am. Chem. Soc.* **2007**, *129*, 14176.

[204] Y. Li, R. T. Yang, *Langmuir* **2007**, *23*, 12937.

[205] Y. Lee, H. R. Moon, Y. E. Cheon, M. P. Suh, *Angew. Chemie Int. Ed.* **2008**, *47*, 7741.

View Article Online
DOI: 10.1039/D5SE01539A

[206] O. Czakkel, B. Nagy, G. Dobos, P. Fouquet, E. Bahn, K. László, *Int. J. Hydrogen Energy* **2019**, *44*, 18169.

[207] Y. S. Al-Hamdani, A. Zen, A. Michaelides, D. Alfè, *Phys. Rev. Mater.* **2023**, *7*, 35402.

[208] A. C. Chien, S. S. C. Chuang, *Int. J. Hydrogen Energy* **2011**, *36*, 6022.

[209] M. Petkovska, D. Antov, W. Zimmermann, E. Schein, *Thermochim. Acta* **2004**, *415*, 21.

[210] K. . Hughes, S. . Miller, J. . Rodriguez, P. . McWhorter, *Sensors Actuators B Chem.* **1996**, *37*, 75.

[211] C. J. Webb, E. M. Gray, *Int. J. Hydrogen Energy* **2014**, *39*, 2168.

[212] A. V. Neimark, P. I. Ravikovitch, *Langmuir* **1997**, *13*, 5148.

[213] G. Liu, Y. Cheng, L. Chen, M. Dong, W. Sun, C. Wu, Y. Wang, Y. Song, N. Wei, S. Zhang, *Vacuum* **2021**, *192*, 110465.

[214] Y. Chen, Q. Liu, Y. Yan, X. Cheng, Y. Liu, *Carbon N. Y.* **2010**, *48*, 714.

[215] H. Pourrahmani, M. H. Mohammadi, B. Pourhasani, A. Gharehghani, M. Moghimi, J. Van herle, *Sci. Rep.* **2023**, *13*, 18032.

View Article Online
DOI: 10.1039/D5SE01539A

Data Availability Statement

The datasets used and/or analyzed during the current study are available from the corresponding author upon reasonable request.